2005-11-16

Array Analysis of Radio Frequency Interference Cancelation Requirements for a Land Mine Detection System

Devin Baker Pratt
Brigham Young University - Provo

ARRAY ANALYSIS OF RADIO FREQUENCY INTERFERENCE CANCELATION REQUIREMENTS FOR A LAND MINE DETECTION SYSTEM

by

Devin B. Pratt

A thesis submitted to the faculty of

Brigham Young University

in partial fulfillment of the requirements for the degree of

Master of Science

Department of Electrical and Computer Engineering

Brigham Young University

December 2005

BRIGHAM YOUNG UNIVERSITY

GRADUATE COMMITTEE APPROVAL

of a thesis submitted by

Devin B. Pratt

This thesis has been read by each member of the following graduate committee and by majority vote has been found to be satisfactory.

Date	Brian D. Jeffs, Chair
Date	Michael A. Jensen
Date	A. Lee Swindlehurst

BRIGHAM YOUNG UNIVERSITY

As chair of the candidate's graduate committee, I have read the thesis of Devin B. Pratt in its final form and have found that (1) its format, citations, and bibliographical style are consistent and acceptable and fulfill university and department style requirements; (2) its illustrative materials including figures, tables, and charts are in place; and (3) the final manuscript is satisfactory to the graduate committee and is ready for submission to the university library.

Date

Brian D. Jeffs
Chair, Graduate Committee

Accepted for the Department

Michael A. Jensen
Graduate Coordinator

Accepted for the College

Alan R. Parkinson
Dean, Ira A. Fulton College of
Engineering and Technology

ABSTRACT

ARRAY ANALYSIS OF RADIO FREQUENCY INTERFERENCE CANCELATION REQUIREMENTS FOR A LAND MINE DETECTION SYSTEM

Devin B. Pratt

Department of Electrical and Computer Engineering

Master of Science

Land mines are a major humanitarian problem with millions of active mines in place around the world. Since these mines can have little metal in them, novel detection techniques are needed. Nuclear Quadrupole Resonance (NQR) is one such technique. Unfortunately, NQR is highly succeptible to radio frequency interference (RFI). A significant contribution of this thesis is the development of a custom, experimental data acquisition system designed and built specifically for capturing RFI at frequencies significant to NQR land mine detection systems. Another major contribution is the development of data analysis techniques for determining the number of reference antennas required to effectively cancel out RFI at frequencies and in environments typical of an NQR land mine detection system.

ACKNOWLEDGMENTS

First of all, I would like to thank my thesis advisor, Dr. Brian Jeffs, for all of his guidance, support, patience, and dedication with this work. I don't think I could have asked for a better advisor. I would also like to thank the other faculty and staff of the Department of Electrical and Computer Engineering. So many have given selflessly of their time and effort to help me with my thesis and with my education in general. I could not have succeeded without them.

Of course, my greatest appreciation goes to my wife, Allison, and my family. They have been exceedingly patient and encouraging, even when it seemed like I would never finish.

Contents

Abstract **ix**

Table of Contents **xiv**

List of Tables **xv**

List of Figures **xvii**

1 Introduction **1**

1.1 Problem Statement 1

1.2 Proposed Research 4

1.3 Signal Models 6

1.4 Previous Work 7

1.5 Thesis Contributions 8

1.6 Thesis Outline 9

2 Data Acquisition System **11**

2.1 System Requirements 11

2.2 Antennas and RF Boxes 12

2.3 Receiver Boards 16

2.4 A/D Cards and Computer 25

3 Field Tests **27**

3.1 System Setup 27

3.2 Data Collection 32

3.3 Calibration of the Array 34

4 Analysis Methods **37**

4.1 Introduction 37

4.2 Data Model 37

4.3 Overview of Analysis Techniques 38

4.3.1 Eigen Analysis 38

4.3.2 Adaptive Cancelation 40

4.4 Simulations of Eigen Analysis and Adaptive Cancelation Techniques . 43

4.5 Preliminary Investigations 50

4.5.1 Statistical Stationarity 51

4.5.2 Reference Channel Ordering 57

4.5.3 Primary Channel Choice 66

4.5.4 Signal of Interest 68

4.5.5 Criteria for Determining the Number of Reference Channels Needed 68

5 Analysis Results **73**

5.1 VRAC Results 73

5.2 Number of Interferers and Reference Antenna Spacing 85

5.3 Interferer Bandwidth 85

5.4 Summary of Results 86

6 Conclusion **89**

Bibliography **91**

List of Tables

2.1 Channel balance measurements. Settings: GC = 0.3V, LO = 23 dBm at 2.842 MHz, input power = -50 dBm. 24

3.1 Field experiment equipment table 28

4.1 $\hat{K}_{VRAC}$ for various block sizes using a threshold of 2% 56

5.1 Summary of $\hat{K}_{VRAC}$ results 81

5.2 Summary of $\hat{K}_{VRAC}$ results excluding clipped data 84

List of Figures

1.1 AP landmine 1
1.2 QM Landmine Detection System 3
1.3 Ionospheric skip 5
2.1 Block diagram of data acquisition system 12
2.2 Antenna array geometry diagram 14
2.3 Comparison of two loop-stick antennas 15
2.4 Schematic of circuit card in RF box 16
2.5 RF box 17
2.6 Antenna mounted to RF box 18
2.7 Block diagram of receiver channel 19
2.8 Schematic of one receiver channel 21
2.9 Box containing the receiver system 22
2.10 Contents of receiver box 22
2.11 Rackmount 23
3.1 Field experiment site 28
3.2 Workstation in trailer 29
3.3 Builders level 30
3.4 Antenna on mast 30
3.5 Cables attached to receiver box 31
3.6 Antenna output 32
3.7 Calibration antenna 35
4.1 Monte Carlo Average $\hat{K}_{AIC}$, $N = 10000$ 43
4.2 Monte Carlo Variance of $\hat{K}_{AIC}$, $N = 10000$ 44
4.3 Monte Carlo Average $\hat{K}_{MDL}$, $N = 10000$ 44

4.4 Monte Carlo Variance of $\hat{K}_{MDL}$, $N = 10000$ 45
4.5 Monte Carlo Average $\hat{K}_{VRAC}$, $N = 10000$ 45
4.6 Monte Carlo Variance of $\hat{K}_{VRAC}$, $N = 10000$ 46
4.7 Monte Carlo Average $\hat{K}_{AIC}$ with random noise power 48
4.8 Monte Carlo Average $\hat{K}_{MDL}$ with random noise power 49
4.9 Monte Carlo Average $\hat{K}_{VRAC}$ with random noise power 49
4.10 Change in covariance over a data frame 52
4.11 Change in covariance over a data frame 53
4.12 Change in covariance over multiple data frames 53
4.13 Average $var(\epsilon_{min})$ for several block sizes 54
4.14 Minimum $var(\epsilon_{min})$ for several block sizes 55
4.15 Maximum $var(\epsilon_{min})$ for several block sizes 55
4.16 Error without reference channel ordering 59
4.17 Error marginal improvement without reference channel ordering . . . 59
4.18 Error with correlation coefficient ordering 60
4.19 Error marginal improvement with correlation coefficient ordering . . . 60
4.20 Error with adjusted reference channel ordering 61
4.21 Error marginal improvement with adjusted reference channel ordering 62
4.22 Radiation pattern of loopstick antennas 63
4.23 Antenna array numbering 64
4.24 Error reduction with orientation ordering 65
4.25 Primary Channel Minimum Error Percent 67
4.26 Primary Channel Minimum Error 67
4.27 Signal of Interest at Carrier 69
4.28 Signal of Interest at baseband 69
4.29 Criteria Example 70
5.1 Mean $\hat{K}_{VRAC}$ for all data frames in second field experiment for primary channel three with threshold = 2% 75
5.2 Minimum $\hat{K}_{VRAC}$ for all data frames in second field experiment for primary channel three with threshold = 2% 75

5.3 Maximum $\hat{K}_{VRAC}$ for all data frames in second field experiment for primary channel three with threshold = 2% 76
5.4 Mean $\hat{K}_{VRAC}$ for all data frames in second field experiment for primary channel six with threshold = 2% 76
5.5 Minimum $\hat{K}_{VRAC}$ for all data frames in second field experiment for primary channel six with threshold = 2% 77
5.6 Maximum $\hat{K}_{VRAC}$ for all data frames in second field experiment for primary channel six with threshold = 2% 77
5.7 Mean $\hat{K}_{VRAC}$ for all data frames in second field experiment for primary channel three with threshold = 5% 78
5.8 Minimum $\hat{K}_{VRAC}$ for all data frames in second field experiment for primary channel three with threshold = 5% 79
5.9 Maximum $\hat{K}_{VRAC}$ for all data frames in second field experiment for primary channel three with threshold = 5% 79
5.10 Mean $\hat{K}_{VRAC}$ for all data frames in second field experiment for primary channel six with threshold = 5% 80
5.11 Minimum $\hat{K}_{VRAC}$ for all data frames in second field experiment for primary channel six with threshold = 5% 80
5.12 Maximum $\hat{K}_{VRAC}$ for all data frames in second field experiment for primary channel six with threshold = 5% 81
5.13 Average $var(\epsilon_{min})$ for all data frames in second field experiment with channel 3 as the primary channel 82
5.14 Average $var(\epsilon_{min})$ for all data frames in second field experiment with channel 6 as the primary channel 82
5.15 Average SINR improvement for all data frames in second field experiment with channel 3 as the primary channel 83
5.16 Average $var(\epsilon_{min})$ for all data frames in second field experiment with channel 6 as the primary channel 84
5.17 Comparison of variance of ϵ_{min} for several adaptive cancelation bandwidths 86

Chapter 1

Introduction

1.1 Problem Statement

Land mines are a major humanitarian problem with millions of active mines in place around the world. They remain hidden long after the conflicts that prompted their use end, finding new victims in innocent civilians. Many in the global community have committed to dealing with this problem by finding and removing these forgotten land mines before they can cause more harm. Unfortunately, this is a difficult and dangerous task. Safe and reliable land mine detection techniques are needed to reduce the risk to those removing land mines and expedite the removal process. The most difficult to detect is the anti-personnel (AP) mine. AP mines (see figure 1.1) are very small (2 to 6 inches in diameter) and can be made from metal, plastic, or wood [1]. It is also becoming more common for anti-vehicle mines to be constructed of non-metallic materials.

Figure 1.1: Photo of an anti-personnel landmine. Photo courtesy United Nations.

The traditional tool for land mine detection has been the metal detector. Unfortunately, metal detectors do not work well with plastic mines, where the only metal might be the firing pin. Sensitivity must be increased to a level at which any metal in the ground would cause a false alarm. This difficulty has prompted the development of other techniques with the hope that they might have a higher probability of detection and be less affected by clutter. Ground penetrating radar and infra-red imaging are two of the methods that are currently being developed.

Another promising technique is Nuclear Quadrupole Resonance (NQR). NQR functions similarly to Nuclear Magnetic Resonance (NMR) but does not require a strong artificial magnetic field. Radio frequency (RF) pulses are transmitted which disturb the orientation of nitrogen nuclei in the material being examined. As the nuclei return to a lower energy level, they produce a decaying exponential resonant return signal [2]. The resonant frequencies are very specific to the chemical composition, which allows an NQR system to detect and identify explosives like RDX and TNT, as well as other chemicals [3]. For example, TNT and RDX have principle resonant frequencies of 842 kHz and 3.41 MHz, respectively. Since NQR can detect the explosive chemical itself, instead of the casing of the land mine, it is immune to clutter issues that afflict techniques like metal detectors and ground penetrating radar.

As with the other land mine detection techniques, there are a few challenges associated with implementing a system based on NQR. First and foremost, the return signals generated by the explosive material are very weak, comparable to thermal noise. Second, the NQR frequencies for the explosive TNT are found in the AM radio band and RDX frequencies are in a crowded shortwave radio band [3]. As such, NQR detectors are highly susceptible to radio frequency interference (RFI). It is particularly difficult to detect a TNT NQR signal in the presence of strong AM radio signals. Since TNT is such a common explosive, it is very important that such systems be able to reliably mitigate the effect of this interference. Even with these limitations, NQR is promising enough to attract the attention of researchers as a viable land mine detection technique.

Figure 1.2: QM Landmine detection system. The primary sensor is mounted on a boom that extends from the front of the Humvee. The reference antennas are mounted on the top of the Humvee. Image courtesy Quantum Magnetics.

Quantum Magnetics, Inc. (QM), a company located in San Diego, CA, has developed a land mine detection system for the US Army which uses NQR to detect mines containing TNT and RDX. Their system consists of a primary RF coil, auxiliary antennas, a data acquisition module, and a computer. The primary antenna transmits the RF pulses and receives the NQR return signals. The auxiliary antennas receive the RFI only (not the NQR signal) and are used for interference cancelation. The data acquisition module and computer receive and process the signals, removing RFI and detecting the presence of any NQR signals [3]. The entire system is housed on a modified Humvee for portability as shown in Figure 1.2.

QM's land mine detection system has performed well in several field tests [3]. However, it has had difficulties detecting TNT signals, particularly at night, due to the presence of RFI. QM's original RFI mitigation system consisted of three reference antennas: two orthogonal B-field loop antennas (antennas sensitive to the magnetic component of electromagnetic waves) and one vertical E-field monopole (sensitive to the electric component of electromagnetic waves). During daytime operation, this RFI mitigation was crucial to achieving good results. QM's antenna suite and adaptive

cancelation processing were often able to drive RFI levels down to the noise floor and reliable detection was demonstrated. During nighttime operation, however, their system was not always able to cancel out the RFI. Clearly there are differences in the RFI environment at night that present some obstacles to the RFI mitigation system. A better understanding of the daytime-nighttime differences, and the RFI environment in general, is needed so that QM can make system design improvements which enable operation in all of the commonly encountered RFI scenarios.

1.2 Proposed Research

We proposed to Quantum Magnetics and the US Army that an increased understanding of the RFI environment would help QM know how to improve its RFI mitigation system. Several issues were identified for study. The first issue is how many reference antennas are needed to effectively cancel out the interference. Adaptive cancelation algorithms like the one used by QM (a multi-channel LMS adaptive filter) require that the mitigation system use at least as many reference antennas as there are interfering signals (a derivation of this fact is found in the next section). It is likely that during nighttime operation the number of AM radio signals reaching the land mine detection system increased due to the effects of ionospheric skip. During the day, solar radiation ionizes the earth's upper atmosphere. The D layer, the lowest layer of the ionosphere, absorbs AM radio signals. After nightfall, the D layer disappears and AM signals are free to pass onto the higher ionospheric layers, where the signals are reflected back to earth (see Figure 1.3). If the number of AM radio stations reaching the test site increased beyond three due to signals traveling further by skipping off the ionosphere, QM's RFI mitigation system would not be able to remove them all.

Results of field tests performed by QM support this hypothesis. During one of QM's field tests, at the Yuma Proving Grounds (YPG) in Arizona, a steady increase in RFI levels after nightfall was observed. The RFI mitigation system was able to cancel out most of the interference during daytime operation but was overwhelmed at night. Another field test at the Aberdeen Proving Grounds (APG) in New York

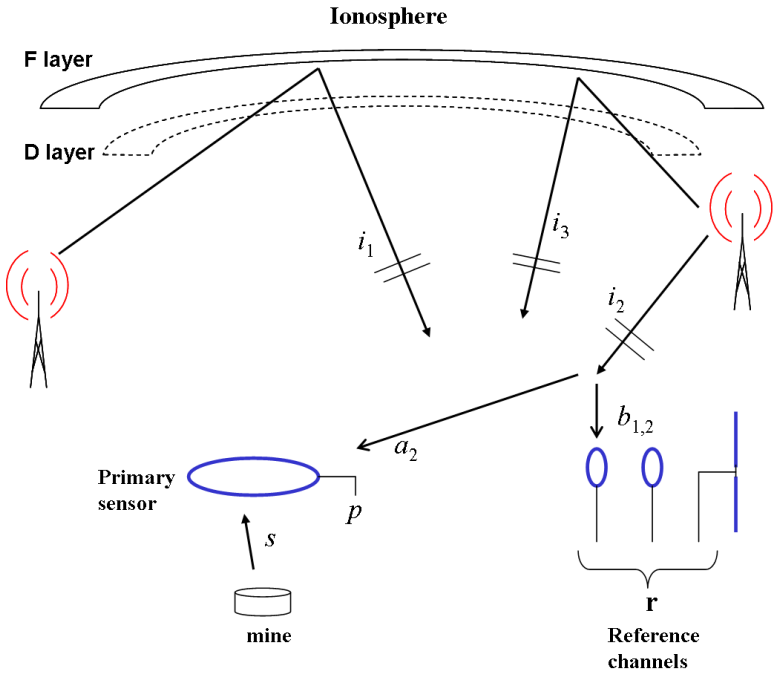

Figure 1.3: Representation of ionospheric skip.

yielded different results. About one hour after nightfall, QM monitored a sudden drop in the RFI levels, after which there was a steady increase in RFI level. This is consistent with the FCC mandated practice of many AM radio stations to drop their power levels at night, precisely because of the ionospheric skip phenomenon. They don't want to interfere with other AM radio stations transmitting at their frequency. In this case, the number of independent interferers might have remained the same as seen during daytime operation. QM's RFI mitigation system was able to cancel out almost all the interference during the day and at night in Aberdeen.

A second issue we proposed for consideration is the importance of spatial sampling over a significant fraction of a wavelength for the reference antennas. Since QM's land mine detection system is mobile and contained on a single truck platform which is electrically very small compared to a wavelength at these frequencies, the reference antennas are essentially co-located and thus provide poor spatial sampling. Achieving sampling at any significant fraction of a wavelength would be a significant

engineering problem. Determining the importance of increased spacing would allow QM to decide if the benefits outweigh the costs.

A third issue deals with the bandwidth of the RFI mitigation system. It is possible that interfering signals whose center frequency is several tens of kHz away from the frequency of interest could contain enough energy in their sidelobes to interfere with reception of an NQR signal. It is possible that by increasing the bandwidth of the RFI mitigation system to include these interfering signals, interference levels at the frequency of interest could be reduced at the canceler output.

We proposed that a custom data acquisition system be designed and built in order to answer these questions. The proposed system will support many channels with elements separated by a significant fraction of a wavelength so that the ideal number of antennas could be determined. A bandwidth greater than that of QM's system is used to determine if increased bandwidth helps RFI cancelation performance. During field experiments, data is collected for at least 24 hours so that any differences in the RFI environment at night can be observed. The acquired data can then be analyzed to determine how many channels are needed for effective cancelation. An analysis of an array covariance matrix computed from acquired data provides some insight into the problem. This thesis is the result of this research proposed to, and accepted by, the US Army and Quantum Magnetics.

1.3 Signal Models

This section presents a model of the signal environment as seen by QM's mine detection system. The minimum number of reference antennas required to cancel out interfering signals is also considered.

The signal at the primary sensor as illustrated in Figure 1.3 is given by

$$p[n] = s[n] + \eta_p[n] + \mathbf{a}^T\mathbf{i}[n], \tag{1.1}$$

where n is the time index, s is the signal of interest, η_p is the noise as seen by the primary antenna, $\mathbf{a}$ is a vector of length L of direction-of-arrival-dependent complex primary sensor gains for each of the interferers, $\mathbf{i}$. The sample index, n, will be

dropped in the following equations for simplicity. The signals seen at the reference antennas, r_j for $j = 1, ..., M$, are:

$$r_j = \eta_j + \mathbf{b_j}^T \mathbf{i}. \tag{1.2}$$

Here, η_j is the noise seen at the jth reference antenna and $\mathbf{b}_j$ is a vector of complex channel propagation gains for each interferer as seen by the jth reference antenna. The vector of reference signals can be expressed as:

$$\mathbf{r} = \boldsymbol{\eta} + \mathbf{B}^T \mathbf{i} \tag{1.3}$$

where $\mathbf{B} = [\mathbf{b}_1, \ldots, \mathbf{b}_M]$ is L x M. An interference cancelation algorithm seeks a vector, $\mathbf{c}$, such that

$$\hat{s} = p - \mathbf{c}^T \mathbf{r} = (s + \mathbf{a}^T \mathbf{i}) - \mathbf{c}^T \mathbf{B}^T \mathbf{i} = s + (\mathbf{a}^T - \mathbf{c}^T \mathbf{B}^T)\mathbf{i} \approx s. \tag{1.4}$$

In order for $\hat{s}$ to equal s, we must have $\mathbf{Bc} = \mathbf{a}$. For arbitrary $\mathbf{a}$ and $\mathbf{c}$ a solution is assured only if $\mathbf{B}$ has full row rank. This requires that $M \geq L$, or in other words, that there be at least as many reference antennas as there are signals of interest. $\mathbf{Bc} = \mathbf{a}$ then becomes a fully determined (for $M = L$) or over-determined (for $M > L$) system of equations in which one or more solutions exist. In the over-determined case, we can find a $\mathbf{c} = \mathbf{B}^\dagger \mathbf{a}$, where $\dagger$ denotes the pseudo-inverse, so that $\hat{s} \approx s$. When there are fewer reference antennas than interfering signals ($M < L$), there aren't enough variables, c_i, to solve all the equations. This is an under-determined system in which all the interferers cannot be canceled. The best we can do is a least squares error solution [4].

1.4 Previous Work

Interference cancelation algorithms typically use adaptive filtering, which is very useful when the statistics of signals and noise are not known a priori or are not stationary. Although it is not commonly used with AM radio RFI, there are many other applications that use adaptive processing with similar signal formulations. Acoustic noise cancelation [5], SONAR [6], and Radio Astronomy [7] all use adaptive

processing to remove interfering signals. The LMS adaptive filter is a particularly common technique because of its simplicity and usefulness across a wide range of applications [8]. In the area specific to AM radio RFI mitigation, Quantum Magnetics has obviously done work [3]. Also, in [9] a frequency domain LMS adaptive filter is used to cancel RFI interference as part of a new land mine detection algorithm for QM's system.

When an array of reference antennas with adequate spatial sampling are available, adaptive array processing techniques can be used to cancel interfering signals. The Multiple Sidelobe Canceller (MSC) described in [10] is particularly appropriate given the signal models in QM's mine detection system. Van Trees [11] provides an overview of several adaptive beamforming algorithms.

1.5 Thesis Contributions

One significant contribution of this thesis is the development of a custom, experimental data acquisition system. The data system was designed and built specifically for capturing RFI at frequencies significant to NQR land mine detection systems. Developing the system required work in a variety of electrical engineering fields, from analog circuit design to both low and high level programming. This flexible and mobile system is capable of acquiring data at both TNT and RDX frequencies using a variety of antenna array configurations.

Field experiments with an experimental system were challenging from both an engineering and logistics point of view. Problems that we encountered were identified, studied, and overcome both during and between the two field experiments.

Another significant contribution is the development of data analysis techniques for determining the number of reference antennas required to effectively cancel out RFI at frequencies and in environments typical of an NQR land mine detection system. Particularly significant is the development, study, and application of the Variable Reference Adaptive Cancelation algorithm. This data analysis was able to determine an estimate of the number of reference antennas required to effectively cancel RFI.

1.6 Thesis Outline

The remainder of this thesis is organized as follows:

Chapter 2, *Data Acquisition Platform*, describes the custom signal sampling system that was designed and built for this project. The system requirement that were established are explained, followed by a detailed description of all the subsystems.

Chapter 3, *Field Tests*, gives a report of two trips to the West Utah desert for data acquisition in a AM RFI environment. The system setup is described as are the procedures followed to collect data. Challenges encountered on the trip and their solutions are also mentioned.

Chapter 4, *Data Analysis*, explains the analysis techniques used to process and analyze the data acquired on the two field tests. Theoretical foundations and test results are given for each method, as are results from the processed data.

Chapter 5, *Conclusions*, summarizes the important results and conclusions from the data analysis.

Chapter 2

Data Acquisition System

A key element of the research for this thesis is the development of a custom, high-speed data acquisition system with which RFI data could be gathered for analysis. This system was designed and built specifically for the purpose of facilitating the investigation of the issues previously identified. It consists of several antennas with associated RF electronics to amplify and filter the received signals before being sampled by an analog to digital (A/D) converter and stored in a computer. Figure 2.1 shows a block diagram of the data acquisition system.

2.1 System Requirements

Several requirements for the data acquisition system were identified. The bandwidth of the system must be large enough to encompass QM's mine detector bandwidth of 50 kHz and also the surrounding spectrum to determine its influence at the frequency of interest. The system must work at the NQR frequencies for both TNT and RDX (842 kHz and 3.41 MHz, respectively). Due to the low power of NQR signals, even weak AM radio stations can interfere with reception. The data acquisition system needs to be able to detect these low level interfering signals. In order to determine the number of interfering signals in a given bandwidth, the system needs to have more antennas than there are signals. Also, the antenna array needs to have sufficient separation between elements so that spatial analysis and filtering can be performed.

The data acquisition system architecture chosen to meet these requirements consists of:

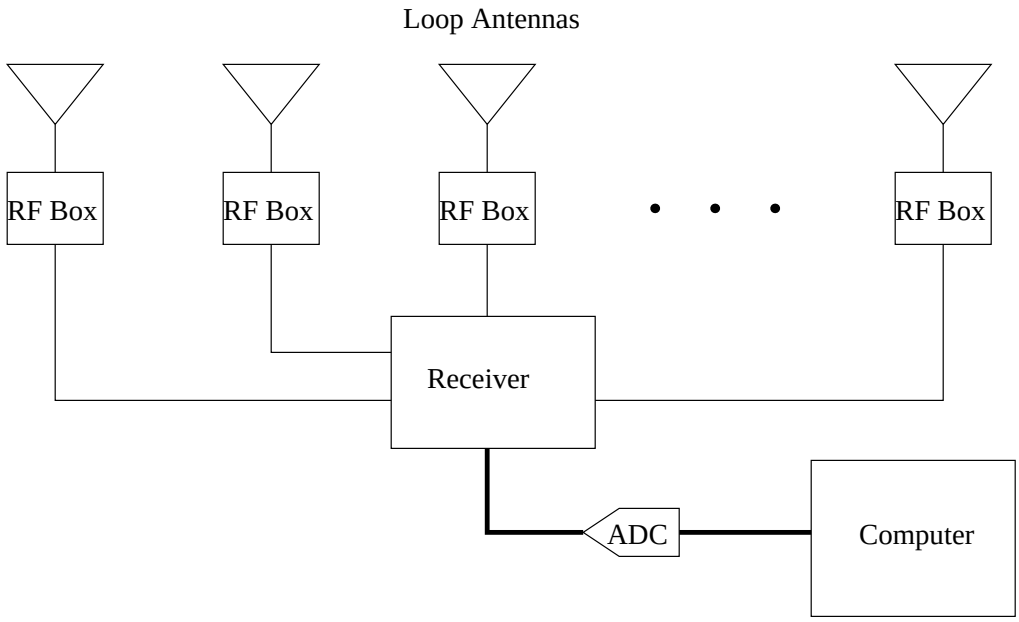

Figure 2.1: Block diagram of data acquisition system

- An array of 12 antennas with local RF boxes to amplify the received signal.
- Receiver boards located at a base station to amplify, mix, and filter the signals.
- A/D cards to sample the data.
- A computer to stream the acquired data to hard disk for storage.

Each of these sub-systems will now be discussed in more detail.

2.2 Antennas and RF Boxes

The receiver system acquisition bandwidth needs to be sufficient to include all the signals that could cause interference at the frequency of interest. However, the sample rate of the data acquisition system is directly related to the receiver's analog bandwidth. In order to guarantee that the data acquisition system can keep up with the incoming bit stream (i.e. samples must be streamed to disk in real-time without data lost), the bandwidth needs to be constrained. Considering all these factors, a bandwidth of 100 kHz was chosen.

The number of antennas was chosen to be 12 to 16 for the following reasons. Allotted frequencies for AM radio stations are separated by 10 kHz, which gives a maximum of 10 local stations in the bandwidth of interest. Often there are fewer than 10. For example, the FCC's AM Radio Database Query (AMQ) lists five stations in the range 790 to 890 kHz in all of Utah. (http://www.fcc.gov/mb/audio/amq.html) At night, however, AM signals can travel further due to ionospheric skip, increasing the number of independent signals received by the array. Twelve to 16 antennas should be enough given all these factors. More than 16 channels would also be very difficult from a data acquisition point of view. At the necessary sample rate we have had to buy the fastest PC host and hard drives available. Since more than 16 channels would exceed the PCI bus data transfer capacity, this would require custom high speed hardware. Due to financial constraints, the first platform revision has 12 channels, but is configured for an easy upgrade to 16.

Antenna spacing in the array must be a significant fraction of a wavelength at the frequency of interest, but preferably close to 1/2 wavelength between adjacent antennas. At 842 kHz the wavelength is 356 m (1169 ft) so achieving half wavelength spacing between all the antennas is logistically prohibitive. A quarter wavelength is 292 ft, a spacing that is both achievable and provides sufficient spatial sampling. Figure 2.2 shows the antenna array geometry used.

In order to meet the design criteria, a sensitive antenna is needed with a passband of 100 kHz. It must be portable (which excluded half wavelength dipoles or quarter wave vertical monopoles, for example). QM's primary sensor is a B-field antenna, and small B-field antennas have better sensitivity than similar sized E-field antennas. This is due to the fact that short vertical E-field antennas have very low radiation resistance and high Q, which leads to poor SNR and narrowband operation. Therefore, it was decided to use a B-field antenna.

After experimenting with several different designs a ferrite loop-stick antenna was chosen. These are composed of wire wrapped around a ferrite core. Many AM radios use this type of antenna, so they were an obvious option. We used larger and higher quality ferrite bars than are found in consumer quality AM radios. Larger

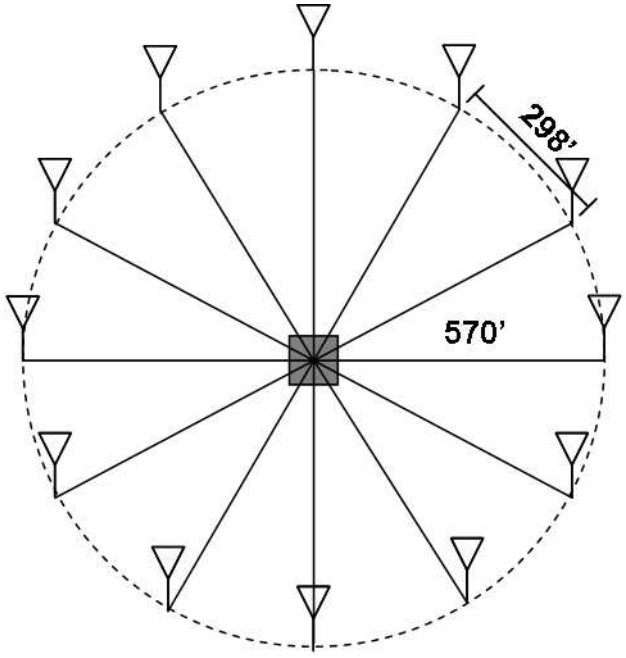

Figure 2.2: Antenna array geometry diagram

ferrite bars have a more effective collecting area and broader tuned bandwidth. They also have lower radiation resistance. Figure 2.3 shows a comparison of a standard AM radio loop-stick antenna and the one used in this project. These antennas have the best bandwidth and sensitivity among several antenna designs tested for this project, and are also very portable.

Our antennas are hand wound. The number of turns must be consistent among all antennas so that their responses are equal. A prototype was built that had good response characteristics and the length of its windings along the ferrite core was measured for duplication. After construction, the inductance of each antenna was measured to see if it matched the prototype. If any deviations were detected, windings were added or removed until a good match was obtained.

A matching network was designed for the antennas to tune them to the correct frequency and match them to 50 ohms. The tuning circuitry contains a variable capacitor which allows the antenna and matching network to be tuned precisely to 842 kHz in spite of variations in the inductance of the antennas and values of the other

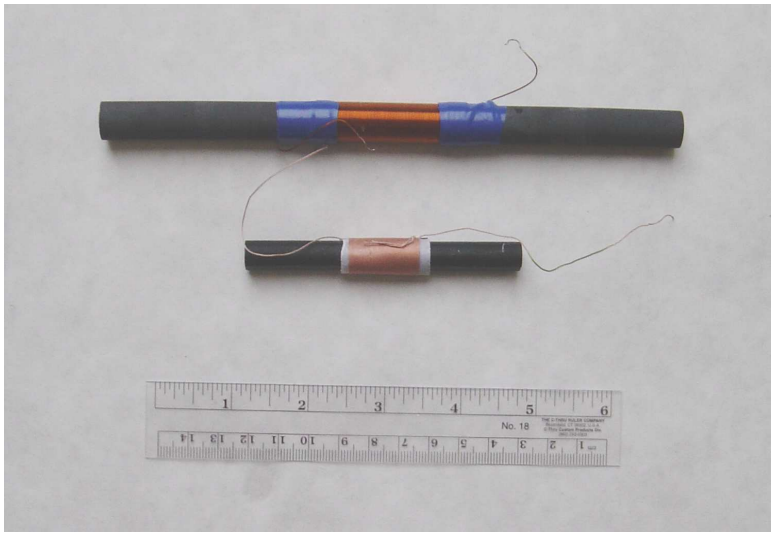

Figure 2.3: Comparison of two loop-stick antennas. The top antenna is the one designed a used for this project. The bottom is a standard AM radio antenna.

capacitors in the matching network. The output of each antenna and matching network pair was examined on a spectrum analyzer and the variable capacitor adjusted with a plastic tuning tool until the passband was centered at 842 kHz.

Since the chosen antennas are high impedance at resonance, a dual stage current amplifier was designed using low noise transistors to match the input impedance of the following low noise amplifier. The 100 K bias resistors at the transistor base serve a dual roll of extending the antenna passband reliably to 100 kHz. A 15 volt power regulator is included to prevent RF noise from entering the system through the power line, and to reduce supply level fluctuations, which are both especially likely because of its long run from the base station to the antenna.

After the circuit design was finalized, a custom PCB for the tuning circuit, current amplifier, and power regulator was designed and milled. Figure 2.4 shows the schematic. This circuit board and the LNA (which serves a dual role as a line driver) are contained in the RF box which is located at the antenna. Figure 2.5 shows a closeup picture of an RF box and figure 2.6 shows a picture of an antenna mounted to an RF box. By having amplifiers located at the antennas the SNR of the signal at

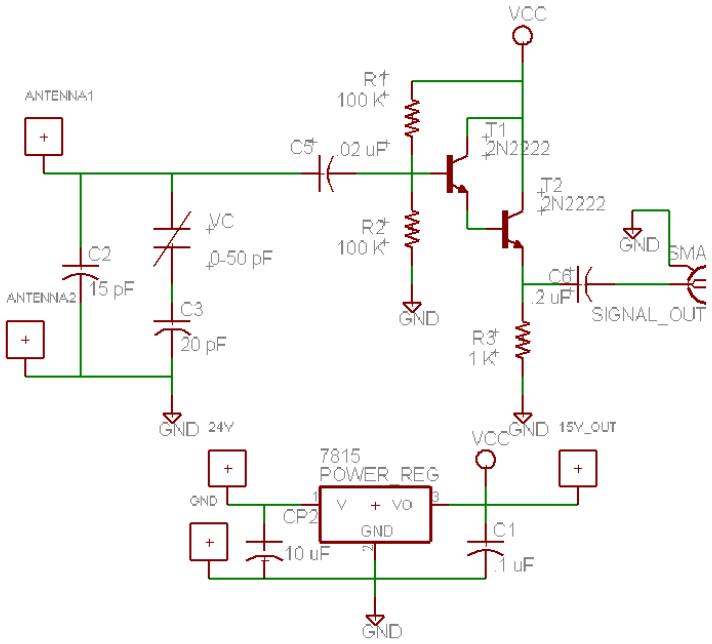

Figure 2.4: Schematic of circuit card in RF box.

the receiver is improved because any noise picked up in the transmission line is less significant compared to the amplified signal of interest. The RF boxes are connected to the base station by coax, which carries the signal, and a single conductor power line, which carries 24 volts to the power regulator. The power supply uses the shield of the coax as a ground reference. Long, insulated standoff support arms for the loopstick and a wood mast pole are used to reduce metallic objects which can distort the B-field near the antenna.

2.3 Receiver Boards

At the base station a circuit is needed to amplify, bandpass filter, and mix the signals received from the RF boxes to an IF frequency suitable for A/D conversion. Since the incoming signal levels were unknown and would likely vary from daytime to nighttime, some form of variable gain control was needed to accommodate as much gain as possible without clipping. Also, the receiver must support both the TNT and

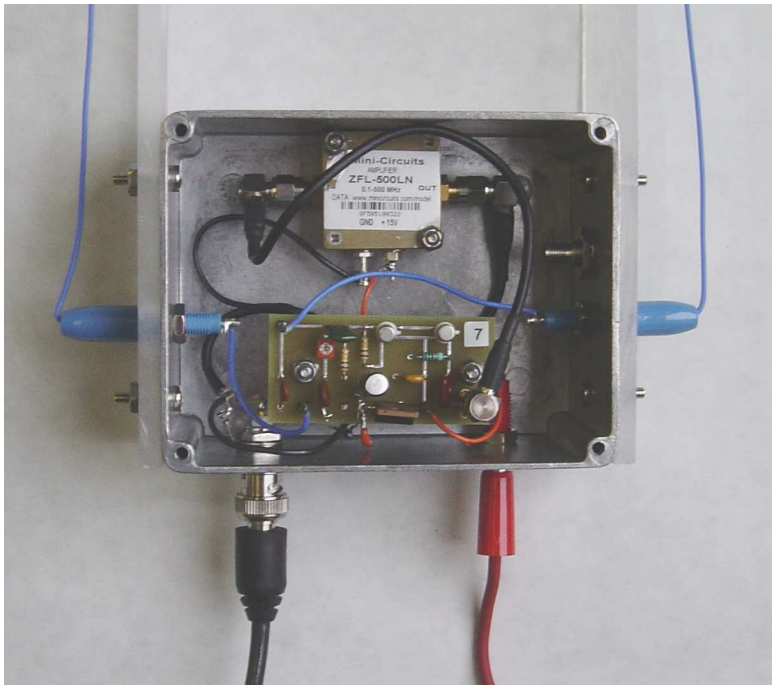

Figure 2.5: RF box. The inputs to the box from the antenna are the connectors on each side. The circuit board at the bottom of the box contains the matching network and current amplifier. At the top of the box is a Mini-Circuits LNA. Coming out the bottom of the box are the signal cable and the power cable which run to the receiver.

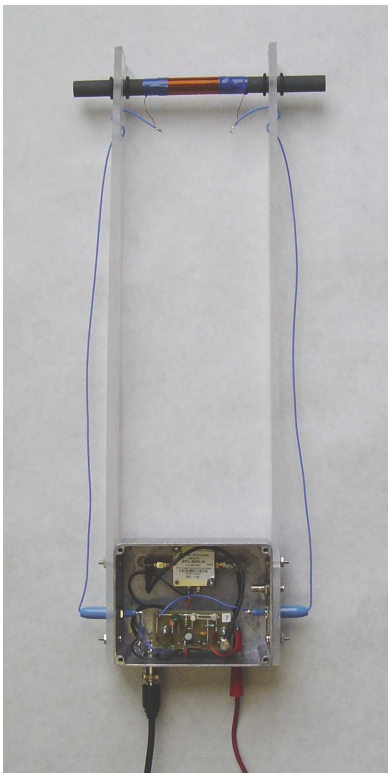

Figure 2.6: Antenna mounted to RF box. Extending up from the RF box are plexiglass struts to which the loop-stick antennas is mounted. It was important to keep the antenna away from any metal because it would affect the antenna's response pattern.

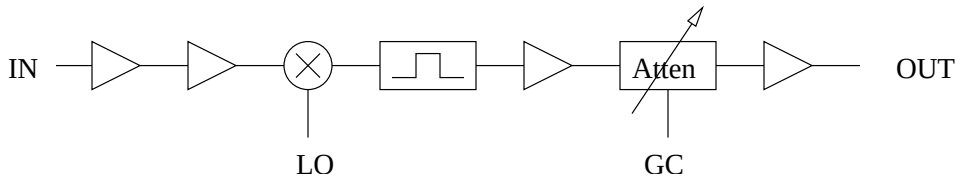

Figure 2.7: Block diagram of a receiver channel. The Local Oscillator (LO) and Gain Control (GC) inputs are shown.

RDX frequencies which means a tunable mixer is required if both are to use the same bandpass filter.

The final receiver design consists of two amplifier stages followed by a mixer and a bandpass filter centered at the intermediate frequency. This is followed by another amplifier, a variable attenuator, and a final amplifier stage. Figure 2.7 shows a block diagram of this architecture.

The Intermediate Frequency (IF) was chosen to be 2 MHz for the following reasons. The IF could not be too close to the TNT or RDX frequencies or the signal images coming out of the mixer would be very close to each other, thus making filtering more difficult and possibly increasing noise aliasing. This requirement, combined with our specified shape parameters for the filter, led the manufacturers to choose 2 MHz as the center frequency of the filter. This allowed them to meet the requirements with as simple a design as possible. The bandpass filter has a 100 kHz passband and 60 dB of attenuation 200 kHz outside the passband. These are custom high grade, high performance, stable filters that were designed commercially specifically for this project to meet requirements and keep uniform performance across the channels.

The variable attenuator used in the receiver is a Mini-Circuits PAS-3. It can be adjusted to attenuate by 2 to 50 dB by varying the voltage on its Gain Control (GC) input. The total gain per receiver channel is 11 to 59 dB, after subtracting losses in the mixer and bandpass filter. Each receiver board consists of four such channels with a common Local Oscillator (LO) input to the mixers and a shared GC input to the variable attenuators. Isolation capacitors and inductors are used to prevent the

coupling of signal into the power traces. A custom PCB was designed and milled for the receivers. Figure 2.8 shows the schematic for one channel on the receiver board.

The four amplifiers for each channel are also from Mini-Circuits. The first and last amplifier stages are MAR-8ASM and the middle two are MAR-4SM. Both parts support frequencies from DC to 1 GHz and can drive up to 12.5 dBm. The MAR-4SM has a gain of 8.3 dB and the MAR-8SM has a gain of 32.5 dB. These are 50 ohm terminated, low cost amplifiers that were very easy to use and supported our modular design criteria. The use of Mini-Circuits microwave modules throughout improved balance between channels and made design and repair easier. Sometimes the gain of an amplifier stage would drop a few dB, creating an imbalance between channels. With the modular design it was easy and cheap to replace the amplifier, which always fixed the problem. Since the amplifiers operate from DC up to 1 GHz, special care had to be taken in design and fabrication to avoid high frequency parasitic oscillations. The 100 pF bypass capacitors at the input of each gain stage effectively suppress parasitics.

The receiver boards are housed in the receiver box, shown in Figures 2.9 and 2.10, which also contains cooling, LO distribution, GC distribution, and power for the receiver boards and the RF boxes. A PC fan provides cooling to the cards and the transformers. A splitter allows a single LO input to the box to be distributed to four receiver boards. A single GC input to the box is also distributed to the receiver boards. One transformer provides the 10 volts for the receiver boards while another transformer sends 24 volts to the RF boxes. The receiver box can also fit in a rack mount as seen in Figure 2.11.

All the receiver channels were measured and tested for balance. Table 2.1 shows the results of a balance test of the three receiver boards. Boards 1, 2 and 3 are the main boards and board 4 contains two backup channels. Because of the variations in the analog parts, Mini-Circuits amplifiers, and bandpass filters, an exact balance was impossible. Any large imbalances were usually due to failed amplifiers (particularly the first stage). The poor performance of board 4 channel 2 is due to its bandpass filter which has a larger attenuation than the other filters.

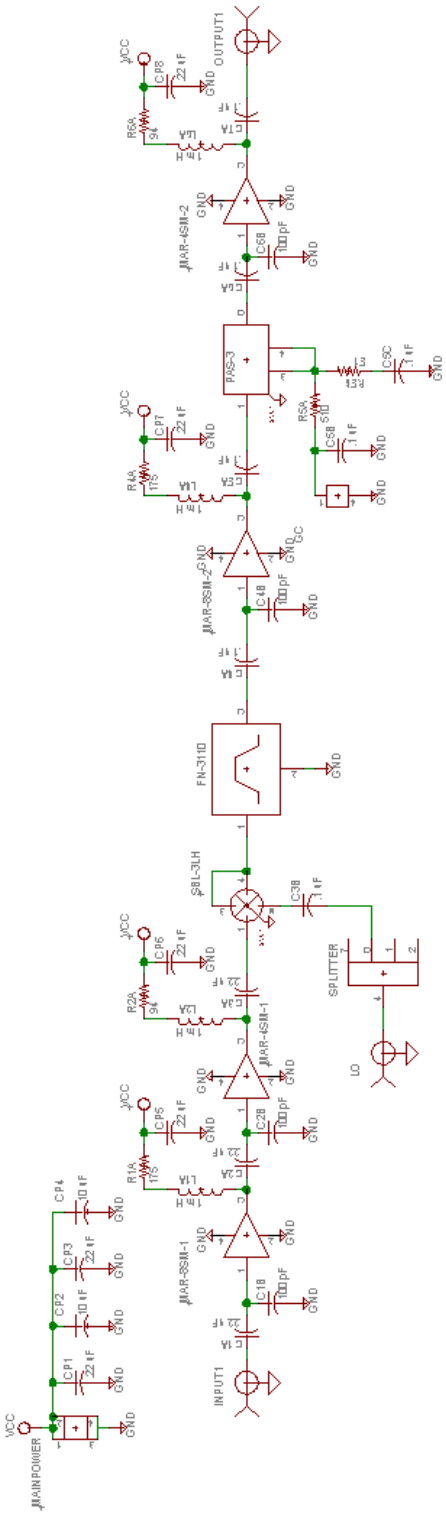

Figure 2.8: Schematic of one receiver channel.

Figure 2.9: Box containing the receiver system.

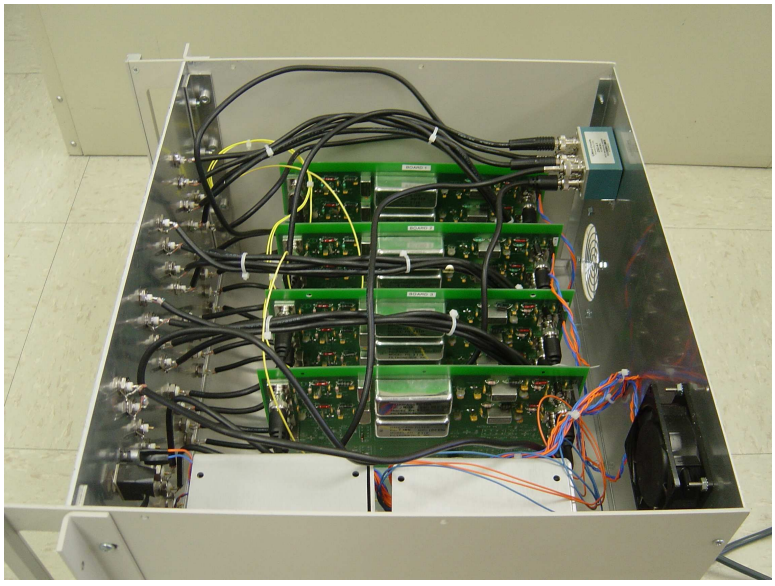

Figure 2.10: Contents of receiver box.

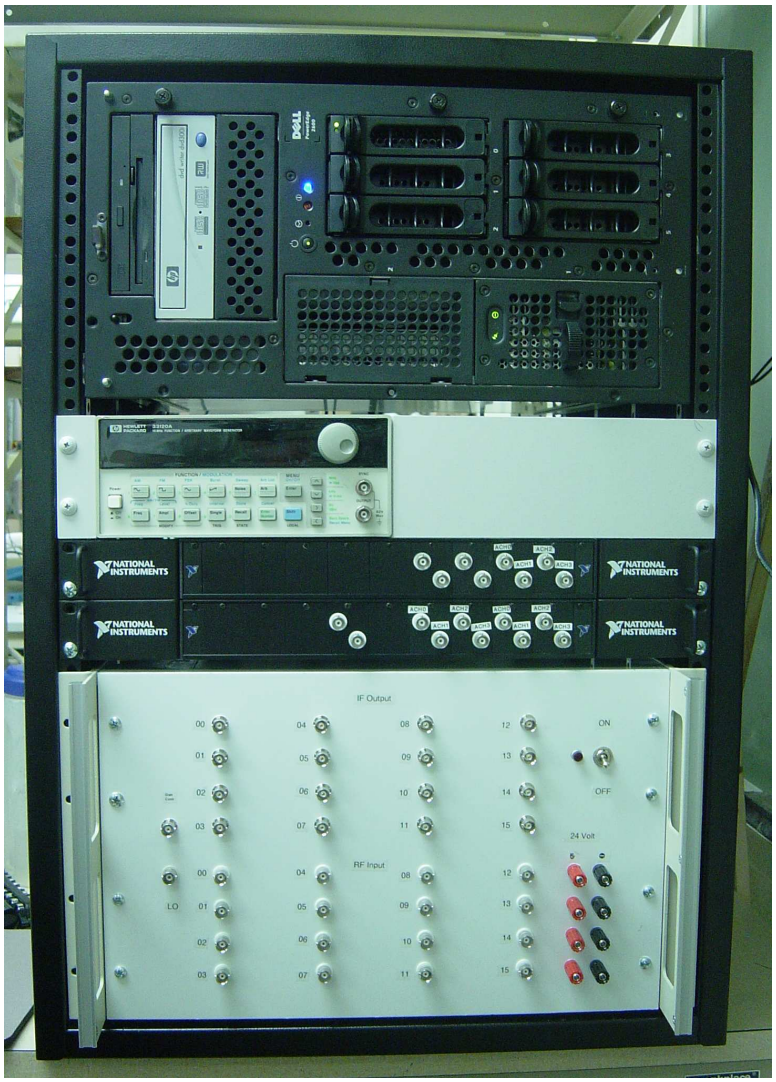

Figure 2.11: At the top of the rackmount is the computer in which the A/D cards are housed. Below that is a signal generator that provides the LO signal. Next are two breakout boxes and the receiver box. The outputs of the receiver box are connected to the A/D cards through the breakout boxes.

Table 2.1: Channel balance measurements. Settings: GC = 0.3V, LO = 23 dBm at 2.842 MHz, input power = -50 dBm.

Board	*Channel*	*Output Power (dB)*
1	1	-17.2
1	2	-17.2
1	3	-19.6
1	4	-20.0
2	1	-18.0
2	2	-21.4
2	3	-17.3
2	4	-18.5
3	1	-17.7
3	2	-19.4
3	3	-18.6
3	4	-18.7
4	1	-21.4
4	2	-24.9

2.4 A/D Cards and Computer

After being amplified, mixed, and filtered, the signal is ready to be sampled and stored. An A/D system is needed that can sample 12 to 16 channels simultaneously and stream the data to hard disk for storage. The A/D card must support sample rates of up to several megahertz, use at least 12 bits in the digitization, and be able to synchronize sampling across several boards. The National Instruments (NI) PCI-6115 10 Msample/sec card was chosen because it satisfies these requirements.

The computer to house the A/D cards must support significant data rates for streaming to disk. The signal at the output of the receiver is centered at 2 MHz and has a bandwidth of 100 kHz. The Nyquist theorem requires that the sample rate be greater than the bandwidth to prevent aliasing. Due to the nature of our signal, bandpass sub-sampling can be used to simultaneously down mix and sample with a minimum sample rate of 200 ksamples/sec as compared to 4.1 Msamples/sec using traditional techniques. Oversampling is helpful because it can increase the distance between images and reduces the effects of aliased noise. Therefore, a sampling rate of 625 kHz was chosen which mixes 2 MHz down to 125 kHz. The nearest image is at -125 kHz and with a 100 kHz bandwidth the edges of the passbands are 150 kHz apart. This gives the bandpass filter plenty of room to attenuate before two images meet. This bandpass subsampling method requires that the A/D cards have analog amplifiers and sample-and-hold circuitry capable of supporting the conventional (i.e. 4.1 Msamples/sec) rates. The NI 6115 satisfies the requirements.

At a sample rate of 625 kHz with 12 channels and 12-bit data, the A/D cards generate 11.25 million bytes (10.7 MB) per second. In order to handle this high throughput, a workstation is needed that has multiple PCI busses and SCSI hard drives. A Dell PowerEdge 2600 with a 2.6 GHz Xeon processor and 1 GB of RAM with 10,000 to 15,000 RPM SCSI drives was chosen.

The data acquisition software to operate the A/D cards and stream the data to disk was written in NI's LabView. The base code came from the High Speed Data Logger (HSDL) virtual instrument (VI) which was developed by NI to read data from an A/D card and write it to disk as fast as possible. The VI has options for various

forms of data compression: no compression (16-bit data words), loss-less compression (12-bit words) and lossy compression (8-bit words). The loss-less compression mode was chosen because it minimizes I/O while preserving the data precision.

HSDL required several enhancements to meet the needs of the project. We modified it to support multiple boards and to synchronize sampling across the boards. Further modifications were made to automate the sampling process. The finished software allows the user to specify how long to sample, how long to wait between sample periods, and how many sampling iterations to perform. The software automatically names the files according to the iteration and stores time, date, compression setting and any user specified information in the header of the data files.

Chapter 3

Field Tests

Once the data acquisition system was built and tested, field experiments were performed to collect data. The first trip was June 3-5, 2004 and the second was September 16-18, 2004. There were two primary requirements for the test site. First, it had to have a large, open, flat area that could fit a circular array of antennas with a diameter of 1140 feet. Second, it had to be far away from the city to reduce RF noise and more closely resemble RF conditions at the test sites QM used. We selected an undeveloped Bureau of Land Management tract north of the Little Sahara Recreation Area in Utah. This is a desert area that is fairly flat and covered with low shrubbery (see Figure 3.1).

3.1 System Setup

In order to accurately place antennas in the configuration of Figure 2.2, surveying equipment was needed to precisely measure distance and angle. A DeWALT builder's level with a 20x magnification scope at the center of the array was used to measure angle relative to the first antenna placed. The other eleven antennas were be spaced at 30 degree increments. A laser rangefinder was used to measure distance from the center of the array to each antenna by using the person placing the antenna as a reflective target. The rangefinder used Nikon ProStaff Laser 440 has a range of up to 400 m, and is accurate to 1 m. This provides position accuracy to within about 0.003 wavelength, which is more than sufficient. The rangefinder also has an optical scope with 8x amplification. Two way radios were used to communicate between the

Figure 3.1: Picture of the field experiment site during the second trip. The calibration antenna and the builders level can be seen at the left. Also shown are the trailer and the two SUVs.

Table 3.1: Field experiment equipment table

Equipment	*Purpose*
12 foot Haulmark Trailer	Used to transport all the equipment and serves as a base of operations. Mobile and rugged enough for light off-roading.
SUVs	Vehicles with off-roading capability were needed to get to the experiment site. It was important to have two in case one got stuck.
Two Honda EU2000 gasoline powered inverters	Provided power for the data acquisition system (through the UPS) and the air conditioner in the trailer.
Pulsar EX2200 RT UPS and Pulsar EXB2200 battery	Supplied clean, reliable power to the data acquisition system. Continuously charged by the generators.

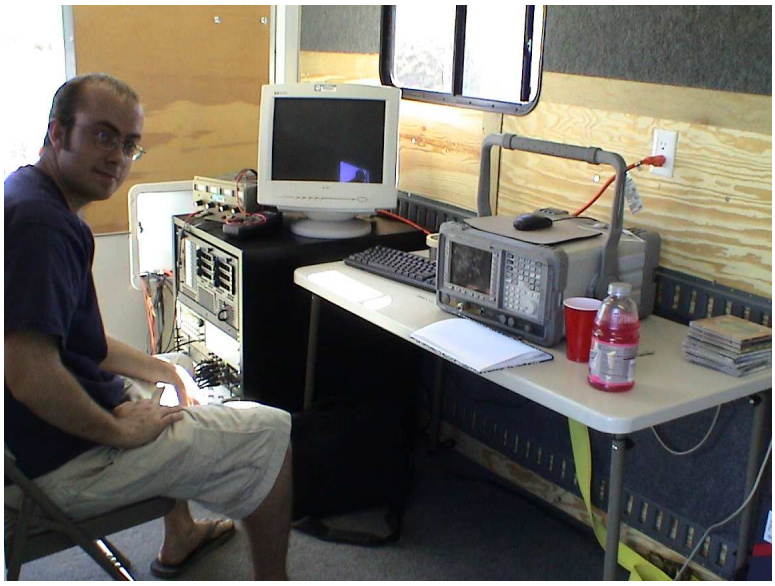

Figure 3.2: Picture of the workstation setup in the trailer from which the data acquisition system was run and monitored.

person placing the antenna and the person at the center of the array measuring angle and distance. The antenna could be guided to the correct location in this manner.

As shown in Figure 3.4, the antennas were mounted on 8 foot wood masts using hose clamps and the masts were attached to ground stakes. Since the loop-stick antennas are directional they needed to be oriented in such a way that the array was sensitive to signals coming from every direction. Each antenna was aligned so that a main response lobe faced the center of the circle. This assured that there were several antennas sensitive to signals coming from any direction. During the second field experiment very high winds caused some of the antennas to rotate. This might have caused decreased sensitivity in some directions.

There were deep gullies at the very edge of the area used for the field experiment. one or two of the antennas could not be placed in their correct location because it was at the bottom of a gully. The closest location at ground level was chosen instead. These deviations, which were always less than 6 yards from the correct

Figure 3.3: Picture of the builders level used to sight the antenna positions.

Figure 3.4: Picture of an antenna mounted on a wood mast. Red flags were attached to increase visibility of the antennas. The reels used to hold the power and signal cable can be seen at the mast base.

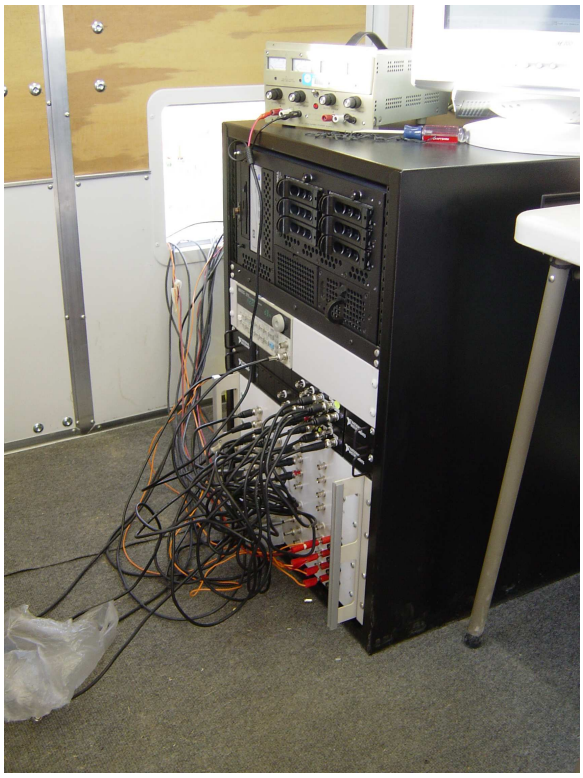

Figure 3.5: Shows all the power and signal cables attached to the receiver box during a field experiment.

location, still preserved 1/4 wavelength spacing and were recorded and included in data analysis.

Power and signal cables were run from the trailer, which housed the rack mount, to the antennas. Each needed its own signal cable, but power cables were shared between pairs of antennas, thus saving a lot of cable and a lot of walking. Figure 3.5 shows signal and power cable connections at the receiver box.

After installation, each channel was tested for proper functionality. Antenna and receiver outputs were examined on a spectrum analyzer to verify that they had the correct frequency response. Then, the data acquisition software was run, and the saved data was examined on the computer to verify proper operation of the A/D cards, computer, and software. Figure 3.6 shows the spectrum analyzer output for

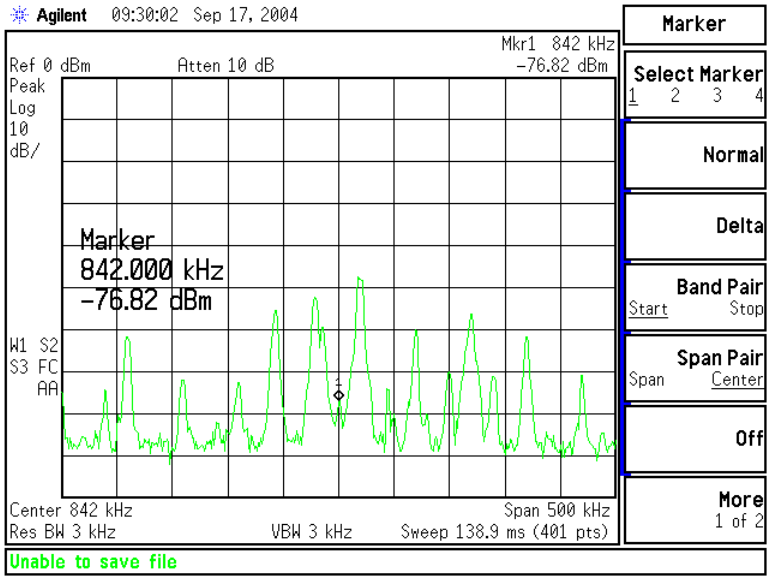

Figure 3.6: Spectrum analyzer screen shot of the output of antenna 1 during the second field experiment. Each peak is an AM radio station.

one antenna during the second field experiment. Note the numerous signals in the tuned antenna passband.

3.2 Data Collection

Quantum Magnetics' mine detection system demonstrated different performance during daytime and nighttime operation, so it was important to run the system for at least twenty-four hours. Any changes in the signal environment corresponding to nightfall could then be detected. In order to record data continuously for twenty-four hours, storage would be needed for $(24 * 60 * 60$ seconds$)*(625000$ samples/second/channel$)*(12$ channels$)*(1.5$ bytes/sample$) = 905$ GB. In order to reduce these hard disk requirements, it was decided to acquire data for one out of every ten minutes, which still provides fairly fine grain time sampling.

Since antennas or receiver channels could fail, it was important to monitor the system for proper performance and implement rapid repair or replacement. BNC connectors on the cables were prone to coming loose and sometimes broke contact.

Also, signal levels tended to rise in the evening and drop in the morning, requiring adjustments in attenuation levels to prevent clipping while maximizing output power from the receiver. The nine minutes of down time between periods of data acquisition were ideal for examining the data stored on the computer. If any problems were detected there, the outputs of the receiver channels and antennas were examined with the spectrum analyzer to determine the source of the problem. Antennas could then be replaced, cable connections fixed, or backup receiver channels used to fix the problem.

One problem encountered during data collection was signal levels were higher than expected. This caused clipping in the receiver even at the maximum attenuator setting (the signals clipped before reaching the adjustable attenuator). We found that with the GC set to 5 volts (minimum attenuation) the maximum input power that does not cause clipping is -70 dBm. With GC set to 0.3 volts, input levels up to -50 dBm could be tolerated (GC levels below 0.3 volts were not used because any differences between GC voltage levels between channels could cause imbalance). Mini-Circuits in-line attenuators HAT-10 and HAT-20 (10 and 20 dB of attenuation, respectively) were brought on the second trip to help prevent clipping. With 30 dB of attenuators per channel, the receiver could handle input levels up to -20 dBm without clipping.

The signal levels were so high that even with the GC set to 0.3 volts, the attenuators were needed the entire second trip, and still there was some clipping. While out in the field it was determined that the power on the LO could probably be turned down without distorting the signals passing through the receiver. The LO power was reduced to 13 dBm instead of the normal 23 dBm in order to alleviate some of the clipping. This was a little risky, but the risk of severe clipping was more pressing. In retrospect, it would have been helpful to go out to the field and measure the signal levels before finalizing the receiver design so that it could be build to match the real signal levels. Signal levels at BYU were measured prior to construction, but were much lower than those observed at the desert test site.

3.3 Calibration of the Array

Calibration of the array was an issue because differences in cable length and analog circuitry, as well as differences in the receiver channels, produced phase and amplitude variations between the channels. In order to calculate accurate correlations it is important to have the channels be as balanced as possible. Corrections can be made during data processing for imbalance if the differences can be characterized. This was accomplished by comparing the channels' responses to a calibration signal sent from the center of the array. An unmatched nine foot vertical antenna was driven by a signal generator which was located directly adjacent to the antenna (see Figure 3.7). The calibration signal was a sinusoid which was transmitted at 842 kHz at 23 dBm. During the second field experiment the frequency of the calibration signal was sometimes set to 845 kHz because there was a relatively strong AM radio station at 840 kHz. By transmitting a few kHz higher, the main passband of the station could be avoided which would make it easier to isolate the calibration signal for analysis. The calibration antenna is a simple, untuned monopole, so energy transfer was not very efficient. But, because it was much closer to the antennas than any other sources, it was the strongest signal in the spectrum.

The calibration coefficient for each channel is computed by isolating the calibration tone in each channel and then computing a cross correlation matrix. Using these calibration coefficients, the channels can be equalized during data processing (calibration is completely explained in chapter 4). During the first field experiment, calibration was only performed twice and the calibration coefficients computed varied significantly. During the second field experiment, the calibration signal was broadcast more regularly, usually once every hour or two, so any changes in the response of the channels could be tracked.

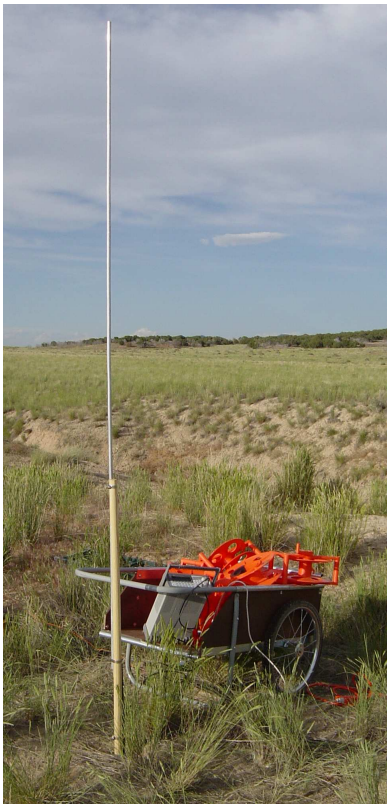

Figure 3.7: Picture of the calibration antenna. The signal generator can be seen just to the right of the antenna.

Chapter 4

Analysis Methods

4.1 Introduction

The purpose of this analysis is to study the issues that we identified in the previous chapter to learn as much as possible about the AM RFI from data gathered during the two field experiments. With this knowledge, Quantum Magnetics will be able to use RFI mitigation techniques that are better adapted to the RFI environment. The primary issue to be addressed is the number of reference antennas needed to cancel out the interference. Other important questions include: how many interfering signals are present, what spacing should the reference antennas have, and what bandwidth of interferers should be included in the RFI mitigation system?

The mathematical model assumed for desired and interfering signals and system are presented in this chapter, followed by a background discussion of the analysis techniques studied. Results of Monte Carlo simulations of the candidate algorithms are presented. A detailed study of the chosen analysis technique is presented that reveals the best settings for working with the data acquired during the field experiments.

4.2 Data Model

The data model for the data acquisition system is similar to the model presented in section 1.3. That model consisted of a primary channel and multiple reference channels. Our data acquisition system does not have a primary channel or

reference channels. Therefore, instead of using p and $\mathbf{r}$ we simply have $\mathbf{x}$. The equations using this slight change in notation will now be given.

The signal environment for our data acquisition system is assumed to consist of K far field interfering sources, i_k for $k = 1, ..., K$, and noise, η, that is spatially and temporally white. The signal received at the m^{th} antenna is then

$$x_m[n] = \eta_m[n] + \mathbf{b}_m^T \mathbf{i}[n], \tag{4.1}$$

where n is the time index, η_m is the noise seen at the m^{th} antenna, and $\mathbf{b}_m$ is a vector of length K of sensor gains for each of the interferers, i_k. In vector form this is

$$\mathbf{x}[n] = \boldsymbol{\eta}[n] + \mathbf{B}^T \mathbf{i}[n],\ \mathbf{B} = [\mathbf{b}_1, ..., \mathbf{b}_M],\ \mathbf{b}_m = [b_{m,1}, ..., b_{m,K}], \tag{4.2}$$

so $b_{m,k}$ is the sensor gain for sensor m to interferer k. These gains are complex and direction-of-arrival-dependent. For simplicity, the time index, n, will not be shown in subsequent equations.

4.3 Overview of Analysis Techniques

This section explains the two techniques that were considered for analyzing the data. The first method is a model order estimate using an analysis of the eigenvalues of the covariance matrix from the acquired data. The second applies an adaptive cancelation technique to evaluate interference reduction as a function of the selection of reference channels.

4.3.1 Eigen Analysis

The problem of determining the number of signals present under the model given in Section 4.2 is one that has been well studied. Under ideal conditions the answer can be determined by simply examining the eigenvalues of the covariance matrix (assuming zero mean random processes) of the data, given by

$$\begin{aligned}
\mathbf{C_{xx}} &= E\{\mathbf{x}\mathbf{x}^H\} = E\{(\boldsymbol{\eta} + \mathbf{B}^T\mathbf{i})(\boldsymbol{\eta} + \mathbf{B}^T\mathbf{i})^H\} \\
&= E\{\boldsymbol{\eta}\boldsymbol{\eta}^H\} + E\{\mathbf{B}^T\mathbf{i}\mathbf{i}^H\mathbf{B}^*\} = E\{\boldsymbol{\eta}\boldsymbol{\eta}^H\} + \mathbf{B}^T E\{\mathbf{i}\mathbf{i}^H\}\mathbf{B}^* \\
&= \mathbf{C}_{\boldsymbol{\eta}\boldsymbol{\eta}} + \mathbf{B}^T\mathbf{C}_{\mathbf{ii}}\mathbf{B}^*,
\end{aligned}$$

where the superscript H denotes the Hermitian transpose and superscript $*$ denotes complex conjugation. Recall that $\mathbf{C_{xx}}$ is M x M, $\mathbf{C_{ii}}$ is K x K, and $\mathbf{B}$ is M x K, where $M > K$.

Let $\mathbf{C_{xx}U} = \mathbf{U\Lambda}$ be the eigen equation for $\mathbf{C_{xx}}$, with $\mathbf{\Lambda} = diag(\lambda_1, \ldots, \lambda_M)$, the diagonal matrix of ordered eigenvalues, and $\mathbf{U}$, the matrix whose columns are the corresponding eigenvectors. Assuming $\mathbf{B}$ and $\mathbf{C_{ii}}$ are both full (column) rank K, then $\lambda_{K+1} = \lambda_{K+2} = \ldots = \lambda_M = \sigma_\eta^2$. $\mathbf{U}_i = [\mathbf{u}_1, \ldots, \mathbf{u}_K]$ spans the interfering signal subspace.

This provides an elegant way to determine the number of interfering signals present in the received data $\mathbf{x}$. $\hat{K}$ is equal to M minus the multiplicity of the smallest eigenvalue of $\mathbf{C_{xx}}$. Unfortunately, in practice the true statistics of $\mathbf{x}$ are not known and must be estimated. Due to sample estimation error in $\hat{\mathbf{C}}_{\mathbf{xx}}$ and the likelihood that $\boldsymbol{\eta}$ is not spatially white, none of the eigenvalues are equal. One might try to simply observe the eigenvalues of $\hat{\mathbf{C}}_{\mathbf{xx}}$ and decide by inspection which of the eigenvalues "should" be equal, but a less ad-hoc approach is preferable.

Two methods for estimating the noise subspace based on information theoretic criteria have been adapted for use in array signal processing by Wax and Kailath [12] and are particularly applicable to this problem. The Akaike Information Criteria (AIC) [13] [14] and Schwartz and Rissanen's Minimum Description Length (MDL) [15] [16] can both be used to estimate the number of signals present based on the eigenvalues of $\hat{\mathbf{C}}_{\mathbf{xx}}$. A very straightforward explanation of how to use these two algorithms can be found in [17].

Both algorithms define criteria for testing a signal model for compatibility with some acquired data. The AIC and MDL criteria are defined, respectively, as

$$AIC = -2 \log f(\mathbf{X}|\hat{\mathbf{\Theta}}) + 2k$$
$$MDL = -\log f(\mathbf{X}|\hat{\mathbf{\Theta}}) + \frac{1}{2} \log N$$

where $\mathbf{X} = \{\mathbf{x}(1), \ldots, \mathbf{x}(N)\}$ is a collection of N observations of $\mathbf{x}$, $\hat{\mathbf{\Theta}}$ is the maximum likelihood estimate of the model parameter vector $\mathbf{\Theta}$, and k is the number of free adjusted model parameters in $\mathbf{\Theta}$. Wax and Kailath derived equivalent expressions for

AIC and MDL using the signal model given in Section 4.2 based on the eigenvalues of $\hat{\mathbf{C}}_{\mathbf{xx}}$:

$$AIC(k) = -2\log\left(\frac{\prod_{i=k+1}^{M}\lambda_i^{\frac{1}{M-k}}}{\frac{1}{M-k}\sum_{i=k+1}^{M}\lambda_i}\right)^{(M-k)N} + 2k(2M-k)$$

$$MDL(k) = -\log\left(\frac{\prod_{i=k+1}^{M}\lambda_i^{\frac{1}{M-k}}}{\frac{1}{M-k}\sum_{i=k+1}^{M}\lambda_i}\right)^{(M-k)N} + \frac{1}{2}k(2M-k)\log N.$$

The λ_i are ordered from largest to smallest $1 \leq i \leq M$. The estimate of the number of signals present in $\mathbf{x}$ is given by

$$\hat{K}_{AIC} = \arg\min_k AIC(k)$$

$$\hat{K}_{MDL} = \arg\min_k MDL(k).$$

The method chosen depends on the the application. Wax and Kailath showed that MDL is a consistent estimator, while AIC is inconsistent and tends to overestimate the number of signals [12]. In [18] it is stated that the lack of the $\log N$ term in AIC allows it to do better with low SNR and smaller N at the cost of being inconsistent. Because MDL has the $\log N$ term, it requires a larger number of observations to work well. Since we have plenty of samples, we prefer MDL.

The eigen analysis technique is attractive because of its simplicity, requiring only the eigenvalues of the sample covariance matrices and N, the number of samples used to estimate them. With an estimate of K we have an indication of how many reference antennas are needed to cancel out all the interferers. There are some practical problems however with AIC and MDL when applied to real world data sets. Some of these issues will be demonstrated in Section 4.4.

4.3.2 Adaptive Cancelation

Another potential analysis technique is based on an adaptive cancelation algorithm used to directly estimate the number of reference channels required to cancel out the interference. We will call this the Variable Reference Adaptive Cancelation (VRAC) algorithm. The concept is to re-run the canceler using a range of reference

antennas, from $m = 1$ through M. The error in the estimate of s, $\epsilon = s - \hat{s}$, is recorded for each set of reference channels. VRAC examines the incremental change in ϵ for each reference channel added. We call the decrease in the variance of ϵ when adding reference channel m the "marginal improvement" for channel m. $\hat{K}_{VRAC}$ is defined as the number of channels used in the adaptive canceler before the marginal improvement goes below a specified threshold or cutoff value (e.g. 1% of the original error). The threshold value is one that can be set by a user as part of a cost-benefit analysis.

Unlike the eigen analysis techniques, this algorithm cannot directly estimate the number of interfering sources. $\hat{K}_{VRAC}$ is an estimate of the number of reference channels required to effectively cancel out the interferers. The case could occur where two interfering signals have the same or almost the same direction of arrival. The adaptive cancelation algorithm would require only one spatial null to cancel both interferers and therefore only one reference channel. Also, poorly spaced or directional antennas can affect $\hat{K}_{VRAC}$. However, $\hat{K}_{VRAC}$ can indicate how many reference antennas the user should have in their RFI cancelation system for best performance in a practical environment.

VRAC is based on an adaptive beamforming algorithm called the Multiple Sidelobe Canceler (MSC) [10]. Van Trees also describes this algorithm as the Wiener-Hopf beamformer [11]. Note that for our analysis, a real-time adaptive cancelation algorithm like LMS is not needed since the data is already acquired and stored, permitting block processing.

The signal model used for this algorithm is as follows. The signal received at the primary channel is

$$p = s + x_1 = s + \eta_1 + \mathbf{b}_1^T \mathbf{i}, \tag{4.3}$$

where we have chosen arbitrarily, and without loss of generality, to designate channel one as the primary channel. s is the signal of interest.

The reference signals, r_m for $m = 2, ..., M$, have a similar model:

$$r_m = \eta_m + \mathbf{b}_m^T \mathbf{i} = x_m. \tag{4.4}$$

In vector form the reference signals are

$$\mathbf{C} = \boldsymbol{\eta} + \mathbf{B}_{\mathbf{C}}^{T}\mathbf{i} = [x_2, \ldots, x_M]^T,\ \mathbf{B} = [\mathbf{b}_1|\mathbf{B}_{\mathbf{C}}]. \tag{4.5}$$

Note the absence of the signal of interest. A crucial assumption for the adaptive cancelation algorithm used here is that the signal of interest not be seen at the reference channels. This is true in QM's scenario because their NQR signal has very low power and can only be detected by their primary sensor. For the data acquisition system used in this project there is no primary channel or signal of interest. Therefore, an artificial source can be added to whichever channel is designated as the primary channel before adaptive cancelation is done.

The MSC algorithm attempts to determine a set of optimum filter weights that can be applied to the data on the reference channels in order to cancel out the interfering signals on the primary channel. The algorithm is

$$\begin{aligned}
&\hat{s} = p - \mathbf{w}^H\mathbf{X}, \\
&\mathbf{w} = \mathbf{C}_{\mathbf{rr}}^{-1}\mathbf{c}_{\mathbf{r}p}, \\
&\mathbf{C}_{\mathbf{rr}} = E\{\mathbf{r}\mathbf{r}^H\},\ \mathbf{c}_{\mathbf{r}p} = E\{\mathbf{r}p^*\}.
\end{aligned}$$

The adaptive beamformer will be able to cancel the interfering signals, $\mathbf{i}$, since they are common to the primary channel and the reference channels. However, it will not be able to cancel the signal of interest, s, since it is not present in the reference channels. The covariance vector $\mathbf{c}_{\mathbf{r}p}$ will only contain information about $\mathbf{i}$, not s. $\hat{p} = \mathbf{w}^H\mathbf{r}$ is a linear minimum mean-square error (LMMSE) estimate of p given $\mathbf{r}$.

Stationarity of the statistics of the observed signals is an important issue for both the eigen analysis technique and the adaptive cancelation algorithm. To this point in the discussion stationary statistics have been assumed (somewhat unreasonably) for $\mathbf{x}$, s, $\boldsymbol{\eta}$, and $\mathbf{i}$. When working with collected data whose statistics are not stationary, the data can be processed by the adaptive beamforming algorithm in blocks. The block size must be small enough so that the statistics are approximately

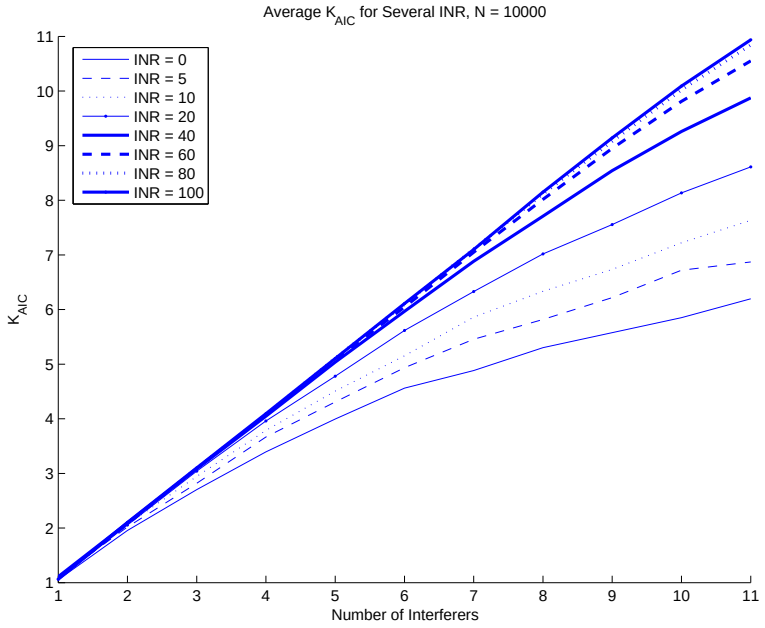

Figure 4.1: Plot of the average value of $\hat{K}_{AIC}$ verses the number of interfering sources for several INR levels using 10000 samples per Monte Carlo trial.

stationary over the whole block, as discussed Section 4.5.1. Estimates of the covariance matrices and **w** are computed for each block of data and then applied to the data in that block.

4.4 Simulations of Eigen Analysis and Adaptive Cancelation Techniques

A series of Monte Carlo trials were run to test the performance of the eigen analysis and VRAC algorithms. In these trials, the number of interference sources was varied from one to eleven for several different INR values (total interference power over total noise power across the array). For each trial, the specified number of interfering sources is created as complex Gaussian random data, each with a random direction of arrival. These are received by a circular array where each channel has some random complex gain. Complex Gaussian white noise (CGWN) is added to the receive channels at the specified INR.

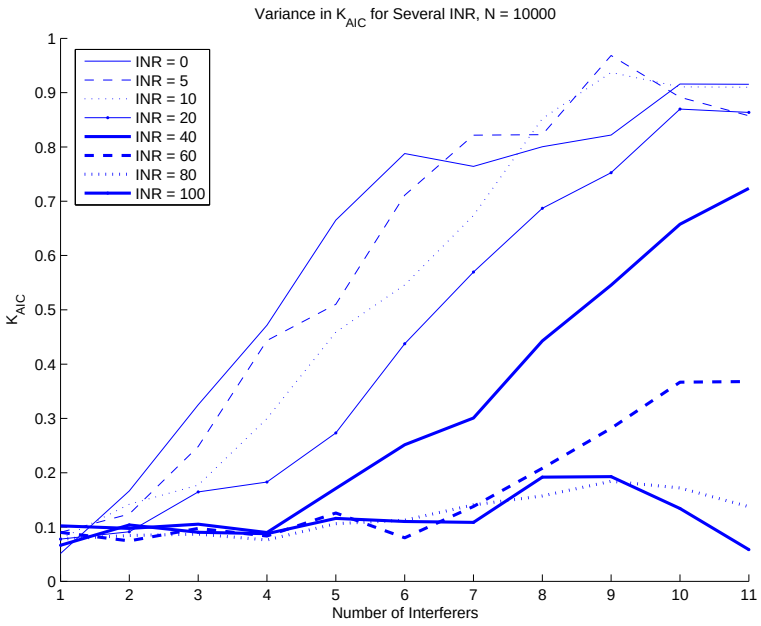

Figure 4.2: Plot of the variance of $\hat{K}_{AIC}$ verses the number of interfering sources for several INR levels using 10000 samples per Monte Carlo trial.

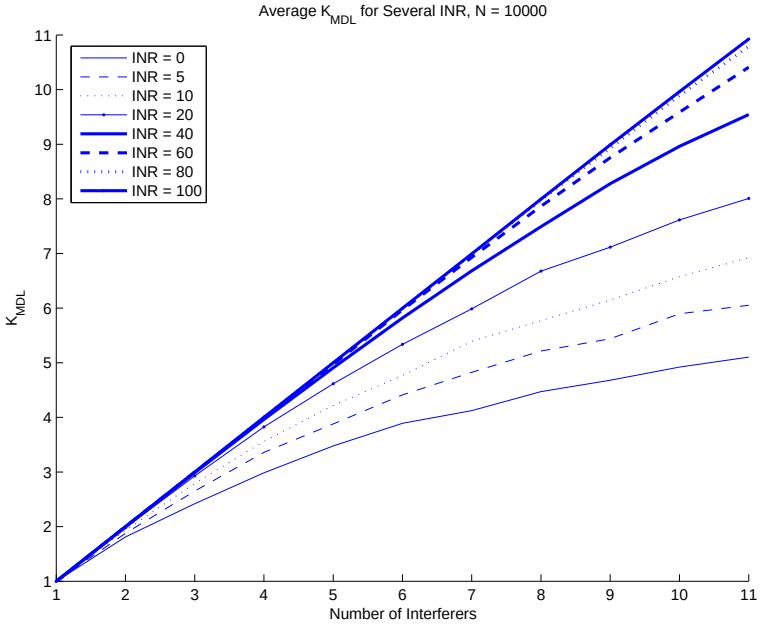

Figure 4.3: Plot of the average value of $\hat{K}_{MDL}$ verses the number of interfering sources for several INR levels using 10000 samples per Monte Carlo trial.

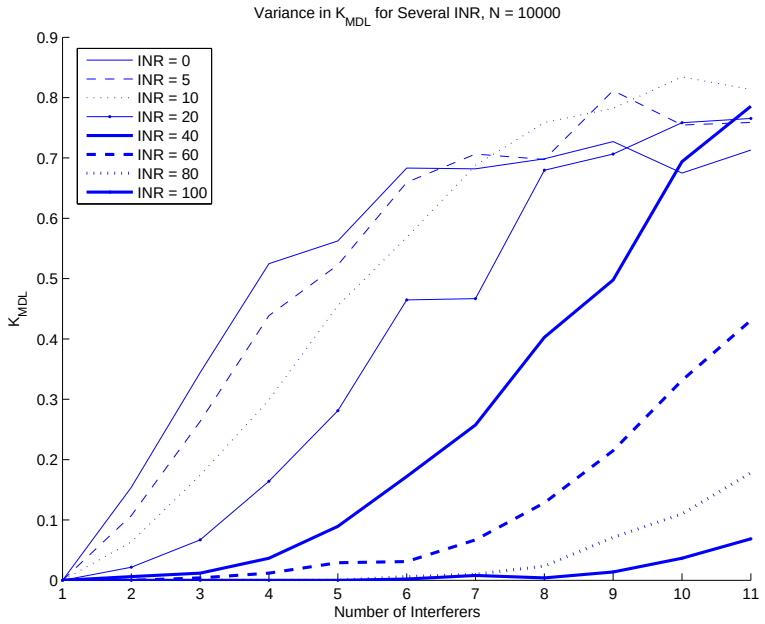

Figure 4.4: Plot of the variance of $\hat{K}_{MDL}$ verses the number of interfering sources for several INR levels using 10000 samples per Monte Carlo trial.

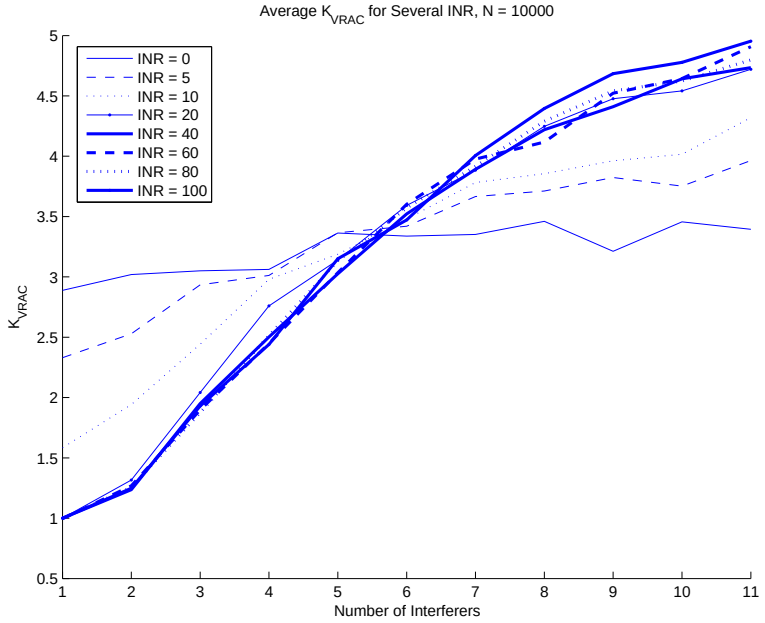

Figure 4.5: Plot of the average value of $\hat{K}_{VRAC}$ verses the number of interfering sources for several INR levels using 10000 samples per Monte Carlo trial.

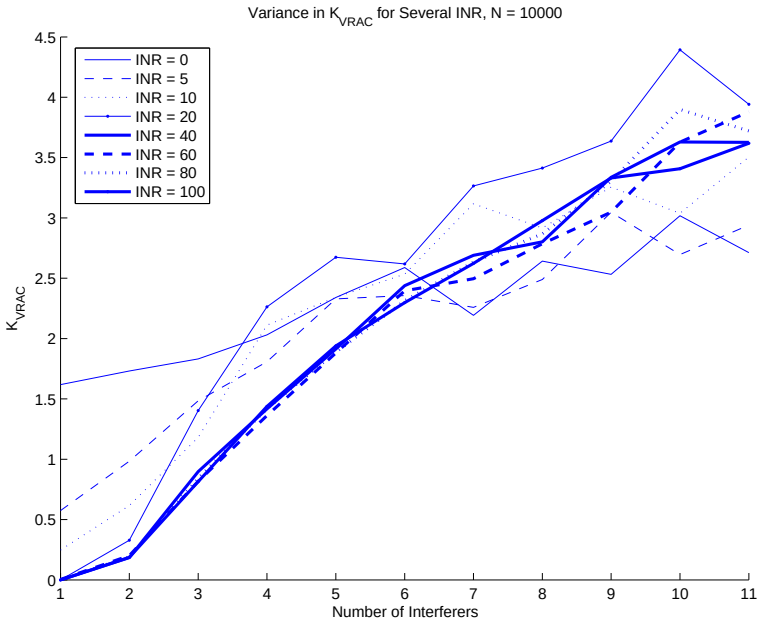

Figure 4.6: Plot of the variance of $\hat{K}_{VRAC}$ verses the number of interfering sources for several INR levels using 10000 samples per Monte Carlo trial.

Figures 4.1 and 4.2 show the average value for $\hat{K}_{AIC}$ and the variance of $\hat{K}_{AIC}$, respectively, using the AIC eigen analysis algorithm. Figures 4.3 and 4.4 show the same for the MDL algorithm and Figures 4.5 and 4.6 show the same for the VRAC algorithm. All of these plots are verses the number of interferers and for INR values ranging from 0 to 100 dB. For these six Figures, 500 trials were averaged and 10000 time samples were used in each trial. The VRAC algorithm was run with a threshold of 1% "marginal improvement".

Figures 4.1 and 4.3 show that even with the idealized signal simulations high INR levels are required to assure good performance of the eigen analysis techniques. On average, an INR of 20 dB is sufficient for AIC and MDL correctly identify up to 4 interferers, 60 dB is required for up to 8 or 9, and and INR of 100 dB is required to identify up to 11 interferers. Figures 4.2 and 4.4 show that the variance of the eigen analysis techniques is also heavily dependent on INR.

Figure 4.5 shows that an INR of 20 dB is sufficient for the VRAC algorithm to achieve its best possible average performance. $\hat{K}_{VRAC}$ consistently underestimates K, but since the end goal is to determine the number of required reference channels, this estimation is the most useful. The asymptotic nature of the plot suggests that no more than five reference antennas would be required to effectively cancel out all of the interference. It should be noted that in the Monte Carlo simulations the antennas were assumed to be isotropic. It is likely that with directional antennas, like the loop stick antennas used in this project, the $\hat{K}_{VRAC}$ values would be higher. Figure 4.6 shows that the variance of this technique is much higher to that of the other and that it is not strongly dependent on the INR. This suggests that in order to get a good mean value for $\hat{K}_{VRAC}$ it is important to use as many trials as possible.

Thus far we've seen that the eigen analysis techniques require high INR values to be able to accurately identify more than a few interferers. VRAC does not have the ability to individually identify very many interferers, but is able to give consistent performance with a lower INR than the eigen analysis techniques. In other experiments (not presented here) it was found that none of the algorithms are terribly sensitive to values of N, although MDL performed noticeably better with more samples.

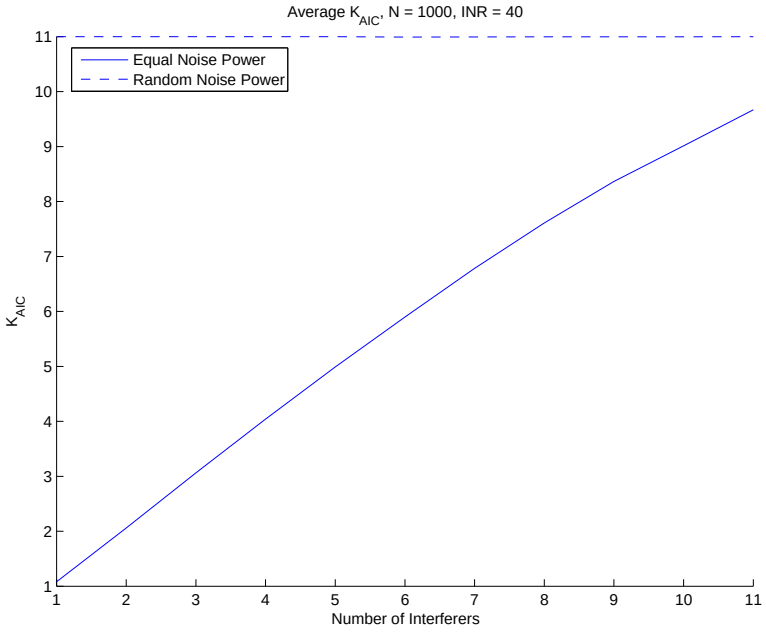

Figure 4.7: Plot of the average $\hat{K}_{AIC}$ verses the number of interfering sources for an INR of 40 dB and $N = 1000$. In this case the noise power across the array was random.

One of the assumptions for the eigen analysis techniques is that the noise power is equal across the array (see Section 4.3.1). This cannot be guaranteed with our data acquisition system, so the effects of white noise that does not have equal power across the array must be investigated. Though noise pre-whitening or generalized eigen-decomposition could be used to correct the problem, this is not practical for our application. It was very difficult to obtain a reliable interference-free noise estimate, as required for these methods. The spectrum, as seen in Figure 3.6, is full of interfering signals, leaving no open bands in which to estimate a noise covariance. The performance of each estimator in the presence of non-white noise is therefore critical to selecting an algorithm. A series of Monte Carlo trials were run with randomized noise power ($\sigma^2_{\eta,m}$) across the array, $N = 1000$, INR fixed at 40 dB, and the number of interferers varied from 1 to 11. Five hundred trials were run for each number of interferers.

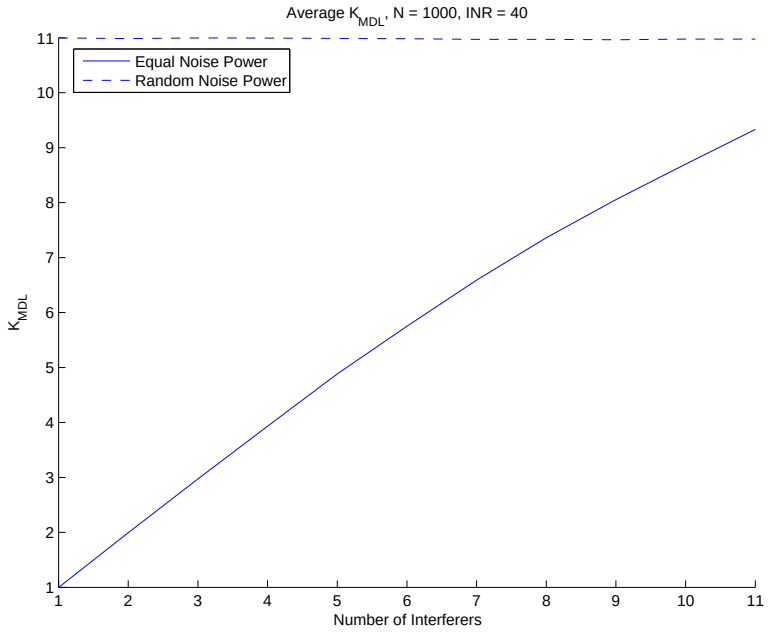

Figure 4.8: Plot of the average $\hat{K}_{MDL}$ verses the number of interfering sources for an INR of 40 dB and $N = 1000$. In this case the noise power across the array was random.

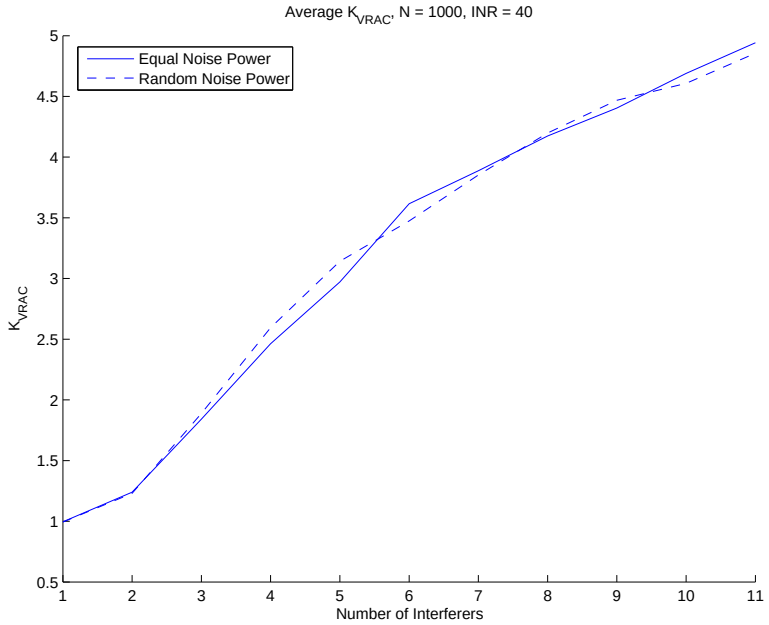

Figure 4.9: Plot of the average $\hat{K}_{VRAC}$ verses the number of interfering sources for an INR of 40 dB and $N = 1000$. In this case the noise power across the array was random.

Figures 4.7, 4.8, and 4.9 show the results for the AIC, MDL, and VRAC algorithms, respectively. In each of these plots, the results for equal noise power are also plotted for comparison. The results for the eigen analysis techniques are striking. For every number of interfering signals, the average estimate of the number of interferers is 11. In some preliminary real data analysis the eigen analysis techniques never returned values of $\hat{K}_{AIC}$ and $\hat{K}_{MDL}$ other than 11. The variances of these estimates (not shown) are well below those when equal noise power was used. The variances in $\hat{K}_{AIC}$ for random noise power are all below 0.009 and the variances in $\hat{K}_{MDL}$ are all below 0.04. The results for the VRAC algorithm with random noise power are almost identical to those with equal noise power, in terms of mean $\hat{K}_{VRAC}$ (shown in Figure 4.9) and variance. This reveals that the VRAC algorithm is much more robust in this respect than the eigen analysis algorithms.

Although the VRAC algorithm does not have the potential of the eigen analysis algorithms to distinguish up to $M-1$ interferers individually, it does provide consistent performance with unequal noise power and at lower INR levels. Its main drawback is the high variance which can only be overcome by using as many estimates of $\hat{K}_{VRAC}$ as possible.

Considering all these factors, the VRAC algorithm is the best choice for providing estimates of the number of reference channels required to effectively cancel out the interference. The rest of this chapter examines the algorithm in more detail so that it might be used as effectively as possible with the data acquired during the two field experiments.

4.5 Preliminary Investigations

There are several settings and parameters for the VRAC algorithm that can greatly affect its performance. This section presents an analysis of these parameters, their effects of the results, and the values chosen for the data analysis. The parameters that require investigation are

- Signal stationarity time.
- Reference channel ordering.
- Primary channel choice.
- The signal of interest.
- Criteria for deciding how many reference channels are needed.

4.5.1 Statistical Stationarity

The adaptive beamformer requires a sample estimate of the covariance matrix of the data, calculated as

$$\hat{\mathbf{C}}_{\mathbf{xx}} = \frac{1}{N}\sum_{i=1}^{N}(\mathbf{x}-\boldsymbol{\mu})(\mathbf{x}-\boldsymbol{\mu})^H. \tag{4.6}$$

For wide sense stationary random processes the error in $\hat{\mathbf{C}}_{\mathbf{xx}}$ is proportional to $1/N$, so it is desirable to make N as large as possible. However, if the statistics of $\mathbf{x}$ are not stationary, then increasing N can increase error by "smearing" the time varying parameters. We will assume that $\mathbf{x}$ is approximately stationary for some length L time window. In this case, the best estimate of the covariance matrix can be obtained by making $N = L$, the size of the largest interval over which the statistics are stationary.

L was determined experimentally. Recall from Section 3.2 that during field experiments data was collected for one out of every ten minutes. Each one minute of data is called a data frame and consists of $60 * 625,000 = 37,500,000$ samples. The stationarity of the statistics were analyzed within several data frames, as was the stationarity across data frames.

For each of the data frames studied, sample covariance matrices were computed in small, 1/2 second blocks. The differences between the covariance matrix estimates were compared using a Frobenius norm to determine over what time period the statistics were approximately unchanging. Differences between each successive $\hat{\mathbf{C}}_{\mathbf{xx}}(l)$ and $\hat{\mathbf{C}}_{\mathbf{xx}}(0)$ from the first 1/2 second block of the data frame are plotted in

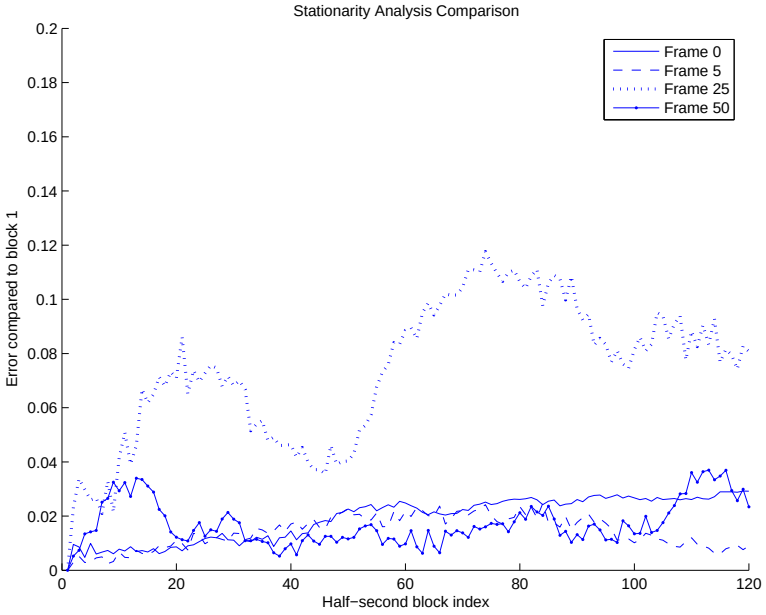

Figure 4.10: Plot of change in covariance matrix for data frames 0, 5, 25, and 50.

Figures 4.10 and 4.11. Figure 4.12 shows a similar plot for data frames that do not contain the calibration signal. Note that all three plots have the same scale on the y axis.

It is clear that the statistics of the signals can change significantly with time. Some data frames (e.g. 5, 125, and 150), seem quite stationary. However, during others (e.g. 25 and 175) the statistics vary significantly. Since the statistics are capable of changing quite drastically, a smaller value for N, perhaps 5 seconds of data, seems appropriate.

Another way to determine the best value for N is to run the adaptive beamformer using different block sizes (i.e. different values of N) and choose the N that gives the best performance. The percent error achieved per block using all 11 reference channel, is the minimum achievable error percentage. Since ϵ was defined as error in the estimate of the signal of interest, we will define ϵ_{min} as the error in the estimate when using all 11 reference channels. By comparing the power or variance of ϵ_{min} for various values of N we can determine the best value.

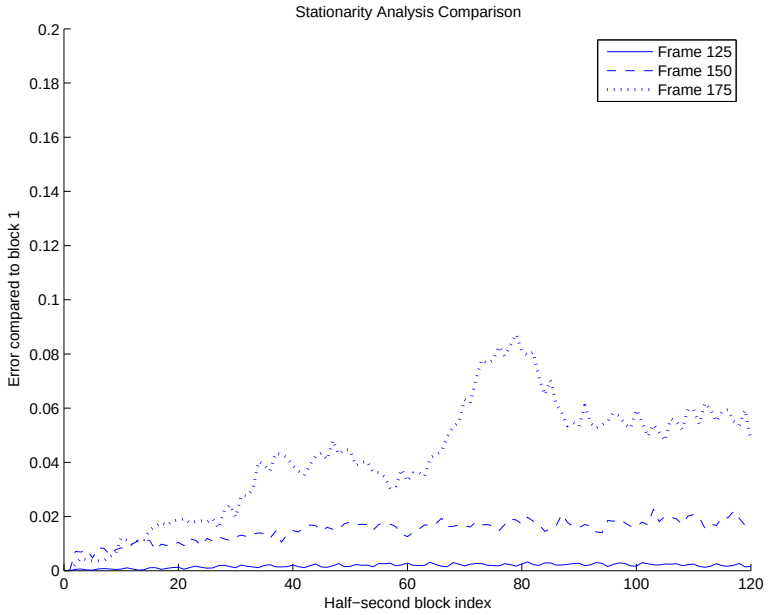

Figure 4.11: Plot of change in covariance matrix for data frames 125, 150, and 175.

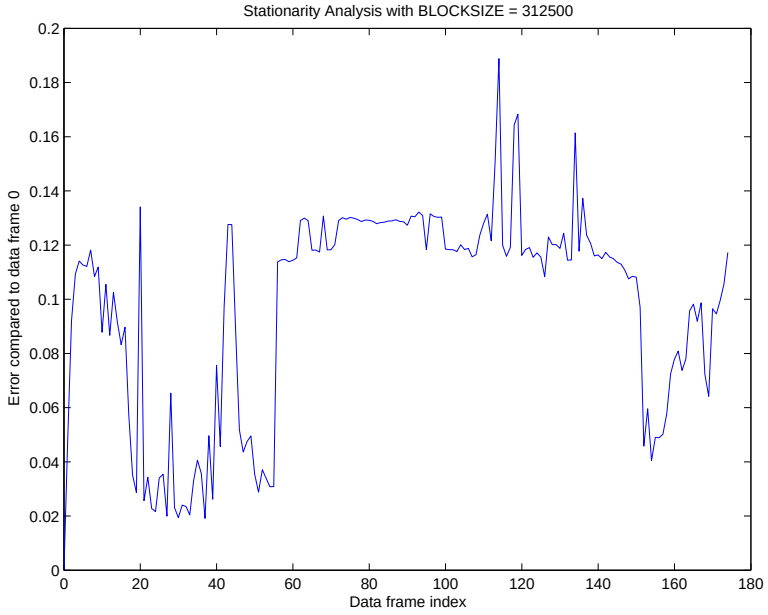

Figure 4.12: Plot of change in covariance over all the data frames that do not contain the calibration signal. Covariance matrices were computed from the first 1/2 second block of data from each data frame. Note that the x-axis shows the index of the data frame in the set of frames without calibration signals, not the frame number.

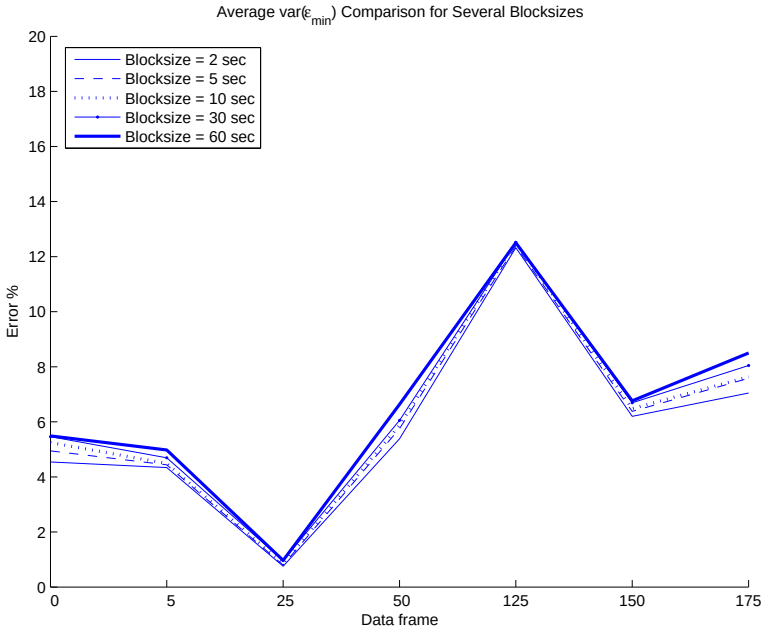

Figure 4.13: Plot of the average $var(\epsilon_{min})$ achieved by the adaptive beamformer using several different block sizes.

Figure 4.13 plots the average $var(\epsilon_{min})$ achieved by the MSC where the average is taken over the blocks in each data frame. This plot shows that smaller block sizes always do better and that the improvement gained by using a smaller block size is at most 2%. Figures 4.14 and 4.15 compare the minimum and maximum $var(\epsilon_{min})$ values for the data frame, respectively. The largest difference in performance for the minimum $var(\epsilon_{min})$ is about 5% and for the maximum $var(\epsilon_{min})$ it is almost 9% (both occur in data frame 175). Note that since there is only one 60 second block per data frame for the 60 second block size, the line for that block size is the same in all three figures and provides a useful point of reference.

These plots would indicate that a large N, say 30 or 60 seconds, might be the best choice. The results from the large block sizes are very close to the average performance of the smaller block sizes. Also, the results do not have the wide variations in performance within a data frame seen with smaller block sizes. The smallest

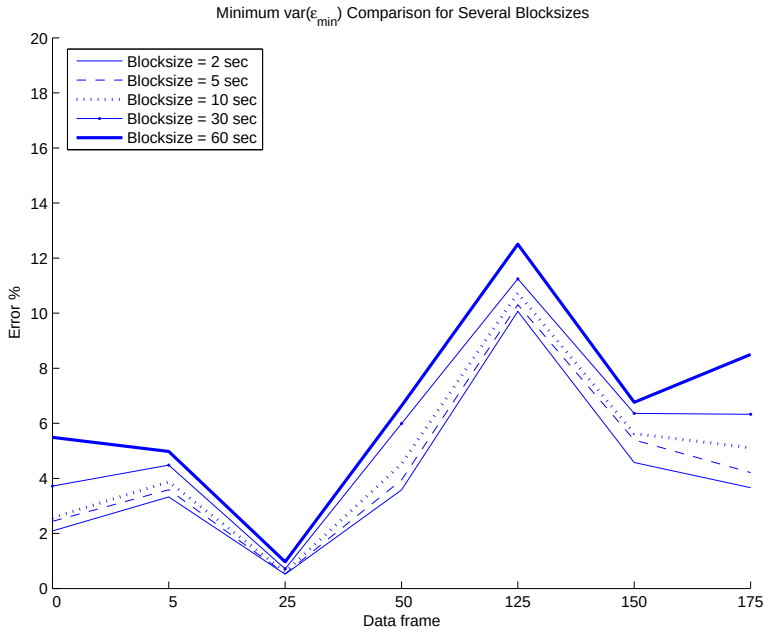

Figure 4.14: Plot of the minimum $var(\epsilon_{min})$ achieved by the adaptive beamformer using several different block sizes.

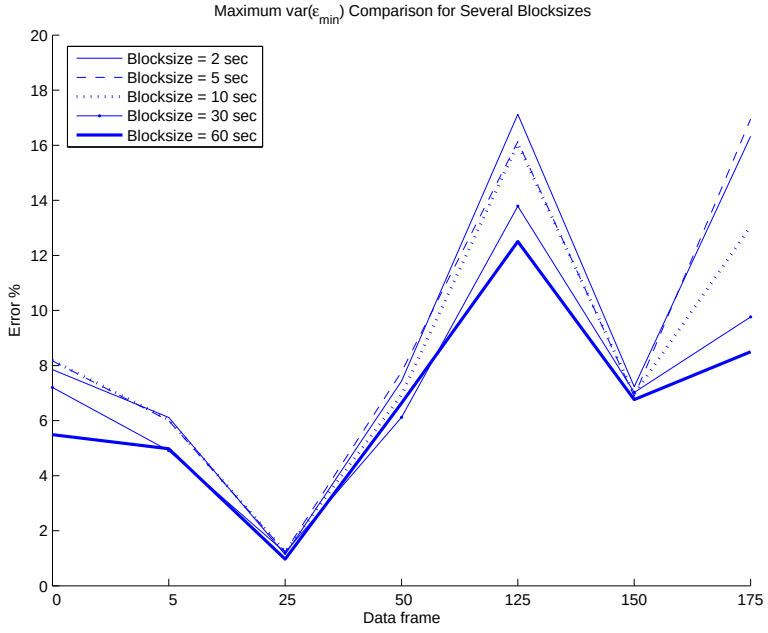

Figure 4.15: Plot of the maximum $var(\epsilon_{min})$ achieved by the adaptive beamformer using several different block sizes.

Table 4.1: $\hat{K}_{VRAC}$ for various block sizes using a threshold of 2%

		Block Size				
		2 sec	*5 sec*	*10 sec*	*30 sec*	*60 sec*
Frame 0	avg	4.43	4.58	4.67	5.50	5.00
	min	2	2	2	4	5
	max	7	7	6	7	5
Frame 5	avg	4.23	4.25	4.17	4.00	4.00
	min	3	4	4	4	4
	max	5	5	5	4	4
Frame 25	avg	1.43	1.42	1.50	1.50	1.00
	min	1	1	1	1	1
	max	2	2	2	2	1
Frame 50	avg	5.37	5.42	5.33	5.00	5.00
	min	3	4	5	5	5
	max	8	7	6	5	5
Frame 125	avg	5.93	6.08	6.00	6.00	6.00
	min	4	4	5	5	6
	max	8	7	7	7	6
Frame 150	avg	4.90	5.50	5.67	6.00	7.00
	min	3	4	4	5	7
	max	7	7	7	7	7
Frame 175	avg	4.50	4.33	4.50	4.50	4.00
	min	3	4	4	4	4
	max	6	5	6	5	4

and largest minimum and maximum $var(\epsilon_{min})$ values, respectively, in these plots are found with the 2 second block size.

In addition to comparing $var(\epsilon_{min})$ for different block sizes, we can consider how many reference channels, as a function of block size, are required to cancel out the interference, $\hat{K}_{VRAC}$. Table 4.1 shows the average, minimum, and maximum values for $\hat{K}_{VRAC}$ for the different block sizes. These values were computed uses a threshold of 2%. For most of the data frames the average values of $\hat{K}_{VRAC}$ are quite similar. Also, smaller block sizes tend to have a larger spread of $\hat{K}_{VRAC}$. This spread could be because the smaller block sizes produce more noisy estimates of the covariance matrices.

It is interesting that the different block sizes do not seem to yield drastically different results from the adaptive beamformer. It is possible that the statistics of the signals are fairly stationary over the whole minute. If so, it appears that even if the estimate of the covariance matrix is better using the whole minute of data, the estimate using just a couple seconds is good enough to reach the noise floor.

The stability of the estimates produced by the larger block sizes is attractive, but so is the ability of the smaller block sizes to better adapt to any variations in the statistics. The Monte Carlo simulations in Section 4.4 showed that $\hat{K}_{VRAC}$ has a high variance which indicates that more results per data frame is important to drive down variance and produce a more accurate average value of $\hat{K}_{VRAC}$. Considering these factors, a block size of 10 seconds is chosen.

4.5.2 Reference Channel Ordering

The VRAC algorithm assumes similar receiver performance across the channels in the data acquisition system. If a reference channel with low gain or INR were used as the first reference channel, it would not be able to cancel out all of the interference that a better reference channel could, and consequently more channels would be required. Quantum Magnetics' reference channels were carefully designed and constructed and likely have a high INR. Therefore, to better approximate the type of response that would be seen with their RFI cancelation system, it is important to use the best reference channels first.

In our data acquisition system the quality of the channels are not equal due to variations in the antennas, the RF electronics, and the receiver. Also, during the field experiments the INR in some of the receiver channels dropped due to amplifiers failing during data acquisition. This discussion is also important when choosing primary channels. For example, if a channel that has completely failed is used as the primary channel, it will not have anything in common with the reference channels. The resulting values for $\hat{K}_{VRAC}$ would be useless. On the other hand, if a channel with a high interference to noise ratio (INR) is used as the primary channel, the adaptive

beamformer will be able to find the interfering signals in the reference channels and cancel them out.

One metric that can help determine the usefulness of a channel is the correlation coefficient. The correlation coefficient between two channels represents how much the two channels have in common statistically. The correlation coefficient for two random variables x and y is

$$\rho_{xy} = \frac{\sigma_{xy}}{\sigma_x \sigma_y}, \tag{4.7}$$

where σ_{xy} is the cross-correlation between x and y and σ_x and σ_y are the standard deviations of x and y, respectively. is $|\rho_{xy}|$ can take on values between 0 and 1, inclusive.

Intuitively, a reference channel whose correlation coefficient with the primary channel is close to one would be more useful in canceling out interference. The reference channels can be ranked by the magnitude of their correlation coefficients with the primary channel, and used in that order. We will call this ordering technique "correlation coefficient ordering." Experimental results have justified this technique, showing that when reference channels are ordered by $|\rho_{xy}|$, more of the error is canceled with fewer reference antennas. Figure 4.16 and 4.18 show the error in the estimate of the signal of interest versus the number of reference channels used, and Figures 4.17 and 4.19 show the percent error reduced (marginal improvement) by each reference channel in the order they were used. The data is the third 10 second block of data frame zero with channel three being used as the primary channel. Figures 4.16 and 4.17 show the results when the reference channels were used in simple numerical order. Figures 4.18 and 4.19 show the results when the reference channels were ordered based on their correlation coefficient with the primary channel.

Correlation coefficient ordering works well, but there are limitations. Sometimes the two highest ranked channels contain the same interference information. Much of the error in the estimate of s is removed using the first reference channel. Adding the second reference channel to the algorithm does not reduce the error by much more because all the useful interference information has been used. Figure 4.19

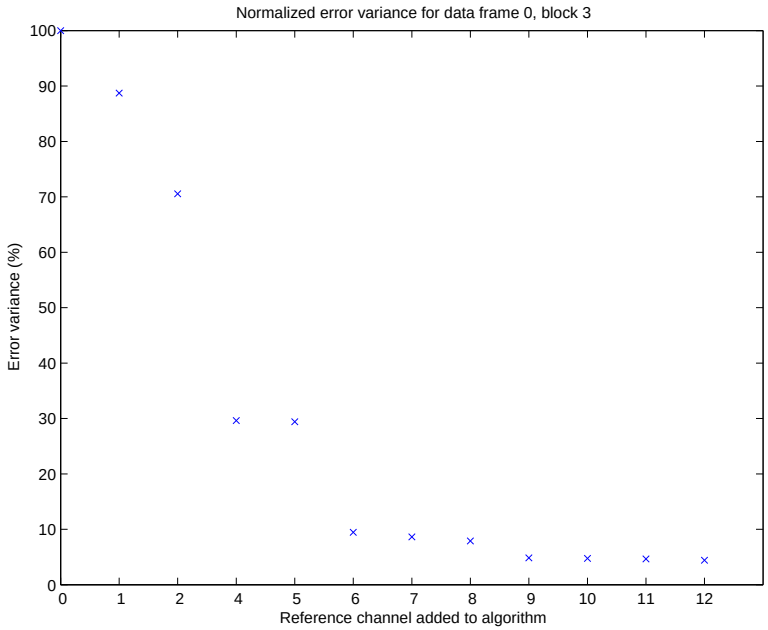

Figure 4.16: Plot of the error of the estimate of s per channel added to the adaptive beamformer algorithm. In this plot the reference channels were used in simple numerical order.

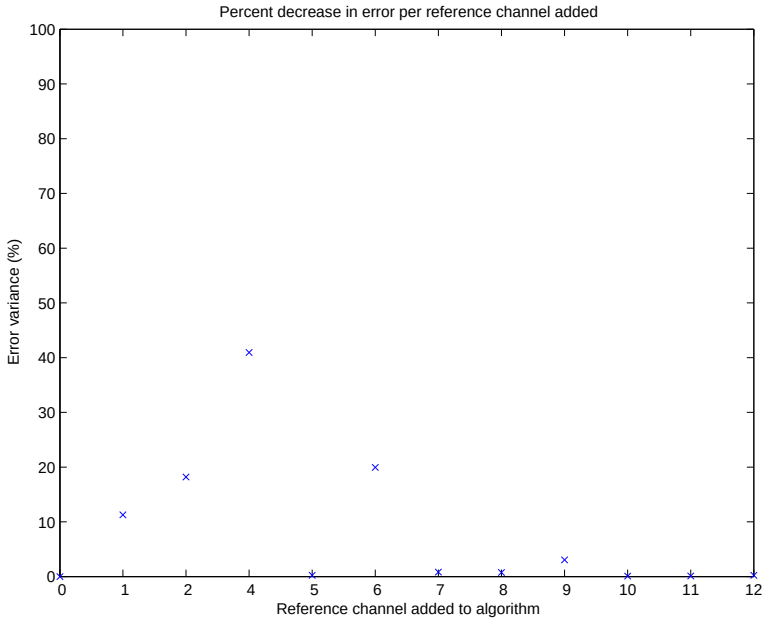

Figure 4.17: Plot of the decrease in the error (marginal improvement) of the estimate of s per channel added to the adaptive beamformer algorithm. In this plot the reference channels were used in simple numerical order.

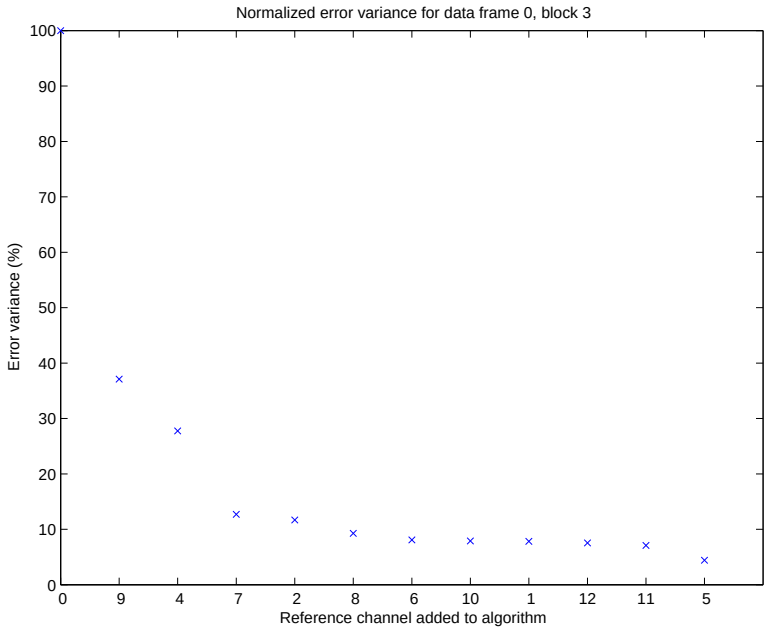

Figure 4.18: Plot of the error of the estimate of s per channel added to the adaptive beamformer algorithm. Correlation coefficient ordering of the reference channels was used.

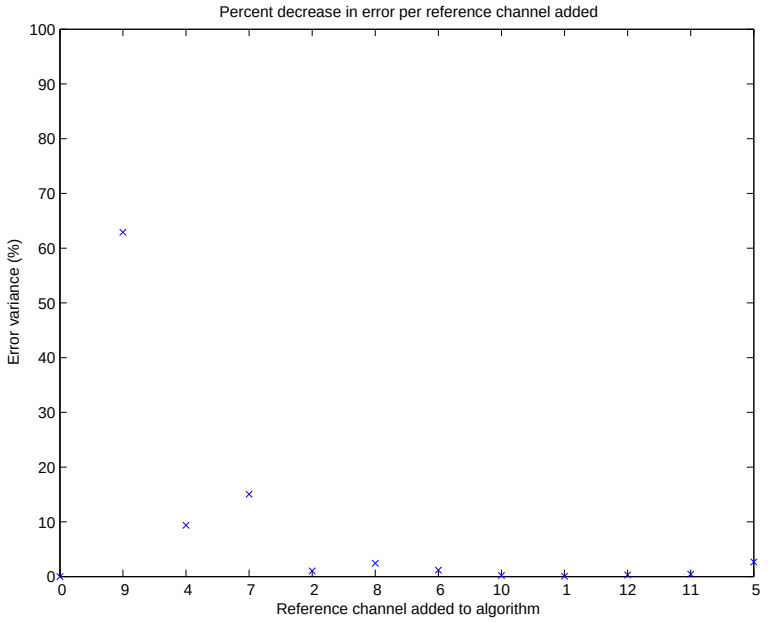

Figure 4.19: Plot of the decrease in the error (marginal improvement) of the estimate of s per channel added to the adaptive beamformer algorithm. Correlation coeffient ordering of the reference channels was used.

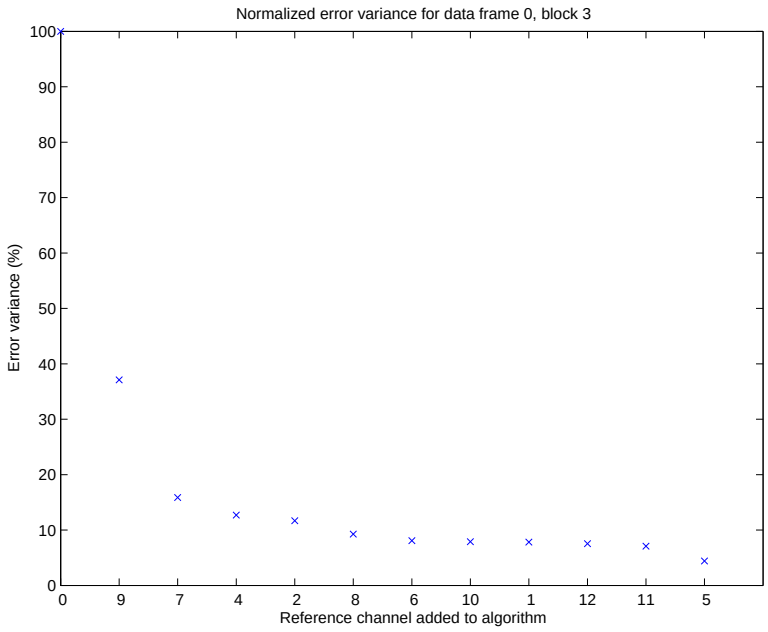

Figure 4.20: Plot of the decrease in the error of the estimate of s per channel added to the adaptive beamformer algorithm. In this plot, the reference channels were used in order of their correlation coefficients except that the second and third channels were switched. Note that the third reference channel contributes very little.

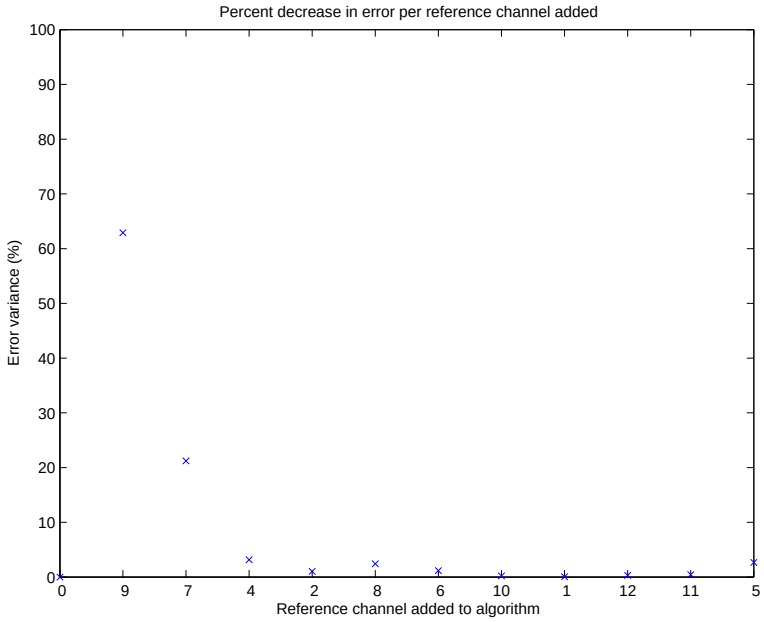

Figure 4.21: Plot of the decrease in the error (marginal improvement) of the estimate of s per channel added to the adaptive beamformer algorithm. In this plot, the reference channels were used in order of their correlation coefficients except that the second and third channels were switched. Note that the third reference channel contributes very little.

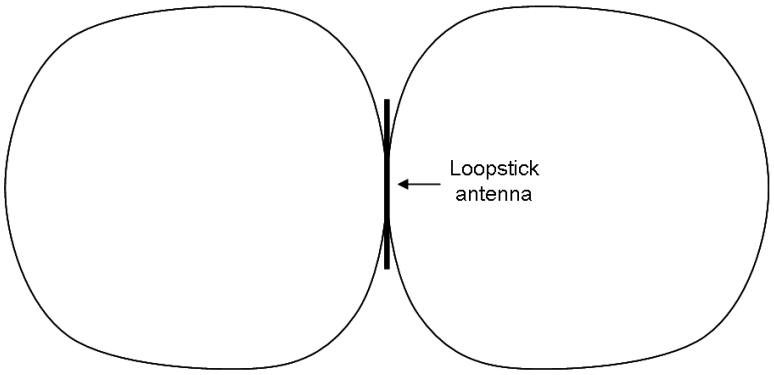

Figure 4.22: Radiation pattern of a small loop antenna, like our loopstick antennas [19]. This is the radiation pattern in the azimuthal plane, looking down on a horizontally oriented antenna.

shows this situation. Figures 4.20 and 4.21 shows the same data processed with an adjusted ordering of the reference channels: the second and third reference channels, numbers four and seven, are switched. In Figure 4.21, the second reference channel contributes more than twice the error reduction as in the previous figure and the third reference channel contributes little. Clearly, even though channel four had more in common with the primary channel, channel seven had more new information.

Another candidate ordering method is based on the orientation of the antennas. The orientation is important because of the directivity of the loop stick antennas. Figure 4.22 shows the radiation pattern of the antennas and figure 4.23 shows the numbering of the antennas in the array. An antenna with the same orientation as the primary antenna would have good INR for the interferers in the direction of the main sidelobe, which would make it a good candidate for the first reference antenna. However, it would be a poor candidate for canceling out interferers that are not in the direction of the main sidelobe. A reference antenna that is oriented perpendicular or almost perpendicular to the primary antenna might be better a choice. Note that in Figure 4.18 and 4.19, the second reference channel chosen by correlation coefficient ranking is channel four which is adjacent to the primary channel, number three. The third reference channel, number seven, is perpendicular to channel four and almost

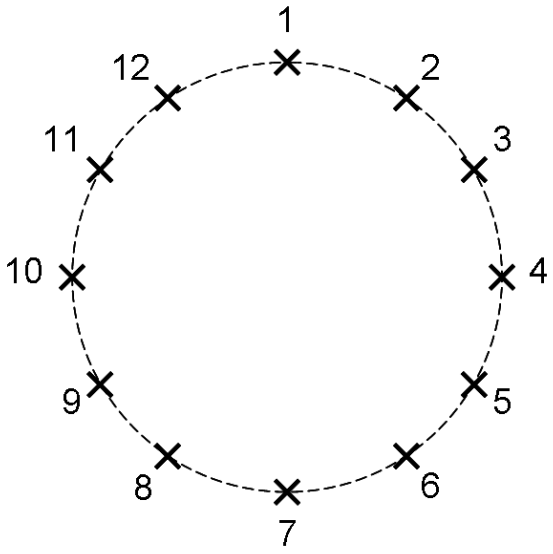

Figure 4.23: Numbering of the antennas in the array based on their position. Antenna one is almost directly north from the center of the array.

perpendicular to channel three. As show in Figures 4.20 and 4.21, it was a better choice for the second reference channel.

This analysis suggests another reference channel ordering technique: reference channels can be ordered based on their orientation. This technique will be called "orientation ordering". The first reference antenna is one with the same or almost the same orientation as the primary antenna. The second antenna is one that is oriented almost perpendicular to the primary. By being almost perpendicular instead of exactly perpendicular, the reference antenna would have its highest sensitivity in a direction at which the primary antenna still had significant sensitivity. The third reference antenna is oriented almost perpendicular to the primary, but in the opposite direction of the second reference antenna. For example, if antenna one is the primary antenna, then the first three reference antennas would be seven, nine, and five. One possible ordering of the rest of the reference antennas is 12, 2, 10, 4, 11, 3, 8, and 6. Note that, in terms of orientation, antenna three is equivalent to nine and eleven to five and can therefore be interchanged.

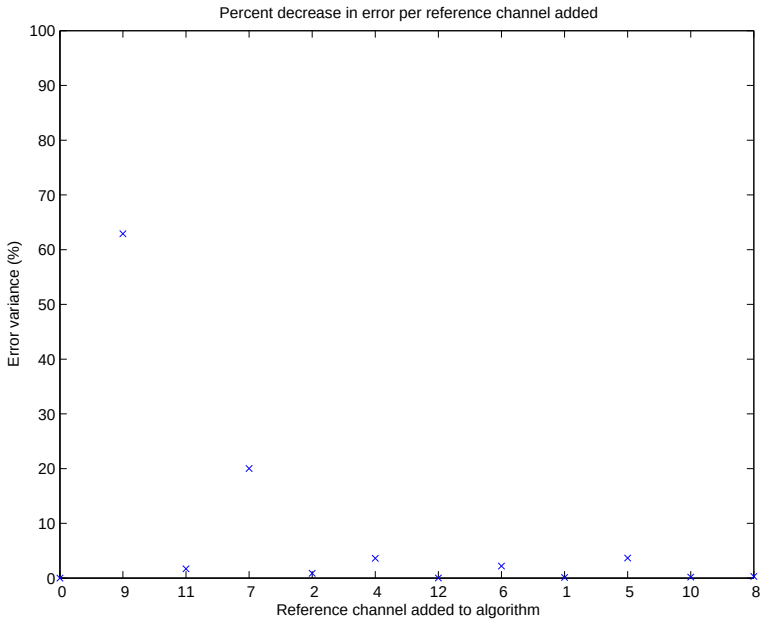

Figure 4.24: Plot of the decrease in the error of the estimate of s per channel added to the adaptive beamformer algorithm. Orienation ordering of the reference channels was used.

Figure 4.24 shows the results from the same data frame and block as before but with orientation ordering of the reference antennas. Here we can see one of the potential problems of this technique. Antennas six and twelve have the same orientation, as do five and eleven. Channels eleven and twelve were used before five and six, yet five and six contributed more to the error reduction. Channels eleven and twelve must have had lower INR. Had a strong interferer been present in the direction of the main lobe of antennas six and twelve, it might have taken both channels to cancel it out if twelve were used first. This would lead us to believe that it takes two channels to cancel out the interference when in fact it only takes one.

As mentioned in Section 3.1, during the second field experiment the windy conditions caused some of the antennas to rotate. The final orientations of the antennas and when they rotated are unknown. Therefore, orientation ordering would be impossible. We can only use this ordering of the reference channels with the data from the first field experiment and the early data from the second field experiment.

Also, the orientation ordering technique assumes that all of the reference chanels are of equal quality. This is not the case with our data acquisition system. Given these two challenges to the orientation ordering technique, correlation coefficient ordering is prefered in general, although orientation ordering might provide some interesting results as well.

4.5.3 Primary Channel Choice

The principal requirement for a primary channel is that it have a high enough INR so that the presence of all the interfering signals can be detected as they are removed by the adaptive beamforming algorithm. A comparison of the minimum error percentage achieved when using each of the twelve channels as the primary channel will reveal which channels have a high INR.

A sampling of data frames taken from throughout the field experiment were used to determine which channels work best as primary channels. The adaptive beamforming algorithm was run separately using each of the 12 channels as primary channels on data frames 0, 10, 40, 140 and 190. One 10 second block was analyzed per frame. The minimum error variance percentage achieved using each channel as a primary channel is shown in Figure 4.25 for each data frame. Figure 4.26 shows a similar plot of the minimum error variance instead of the percent.

Figure 4.25 shows that channels 3, 5, 6, 8, 9, and 10 consistently have the lowest error percentages and work well as primary channels. In Figure 4.26 channels 5 and 12 have particularly high error variances. Since channel 5 also has low error percentages, it is likely that there is simply more gain on channel 5. Channel 12, on the other hand, has high error percentages, which indicates that it has a low INR. Given these results, channels 3, 5, 6, 8, 9, and 10 are all good choices for primary channels.

Due to the directivity of the loopstick antennas any antenna would be insensitive to signals in the end-fire direction. By using two antennas with different

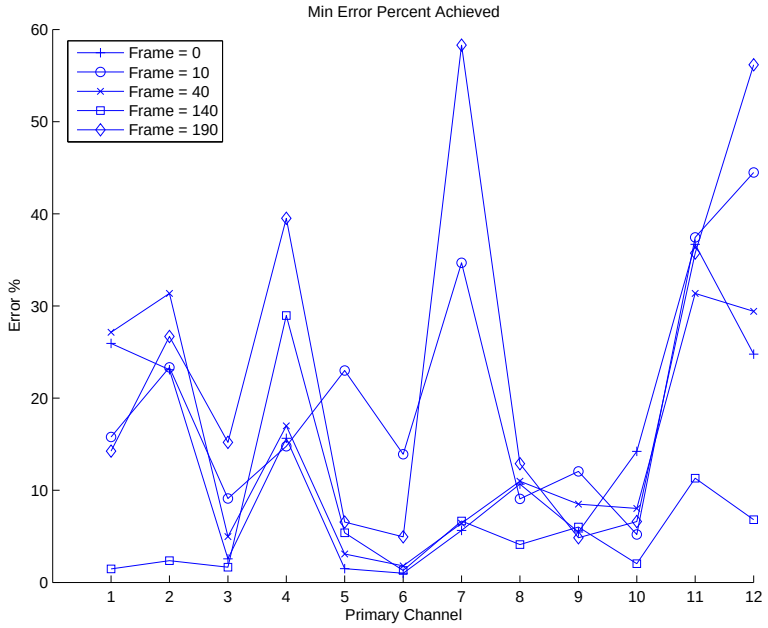

Figure 4.25: Plot of the minimum error variance percent compared to the original error obtained using each of the twelve channels as the primary channel for several data frames.

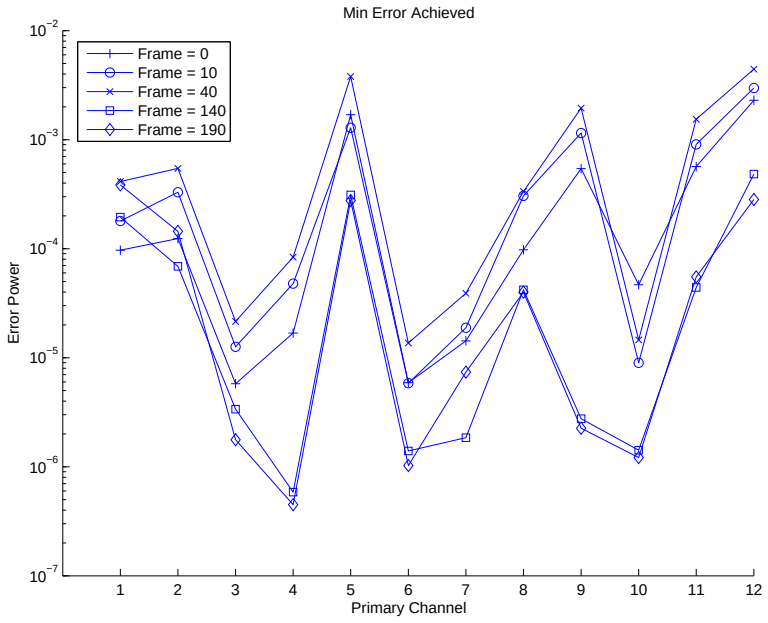

Figure 4.26: Plot of the minimum error variance obtained using each of the twelve channels as the primary channel for several data frames. Note that the y axis has a log scale.

orientation as primary channels, all of the interfering signals can be detected. Channels three and six will be used for most of the analysis since these two are oriented perpendicular to each other.

4.5.4 Signal of Interest

In Quantum Magnetics' land mine detection system, there is a signal of interest, s, that is received at the primary sensor but not at the reference sensors. Since there is no signal of interest inherent in the data acquired from the field experiments, one is added artificially to the primary channel before the VRAC algorithm is applied. This allows us to verify that the adaptive beamforming algorithm is working correctly and not attenuating or distorting the signal of interest.

The NQR return signal is a pulse centered at the NQR frequency for the material modulated by a rising and decaying exponential signal. The exact form and decay times are proprietary information. We generate a signal similar in form to the NQR return. A plot of our signal of interest at the carrier NQR frequency is shown in Figure 4.27. A version of this signal that is mixed down to baseband and low pass filtered is shown in Figure 4.28. This is the signal that is added to the primary channel after the acquired data is mixed and filtered and before the statistics are estimated.

4.5.5 Criteria for Determining the Number of Reference Channels Needed

When analyzing the data, a criteria is needed that determines the number of reference channels required to effectively cancel the interfering signals, $\hat{K}_{VRAC}$. One possible criteria is the one described in Section 4.3.2: the number of channels used in the adaptive beamformer before the marginal improvement goes below a specified threshold or cutoff value (e.g. 1% of the original error variance).

This would be the best criteria if we could guarantee that the reference channels are used in an optimum order. When the reference channels are not used in an optimum order, it is possible that the marginal improvements from one reference

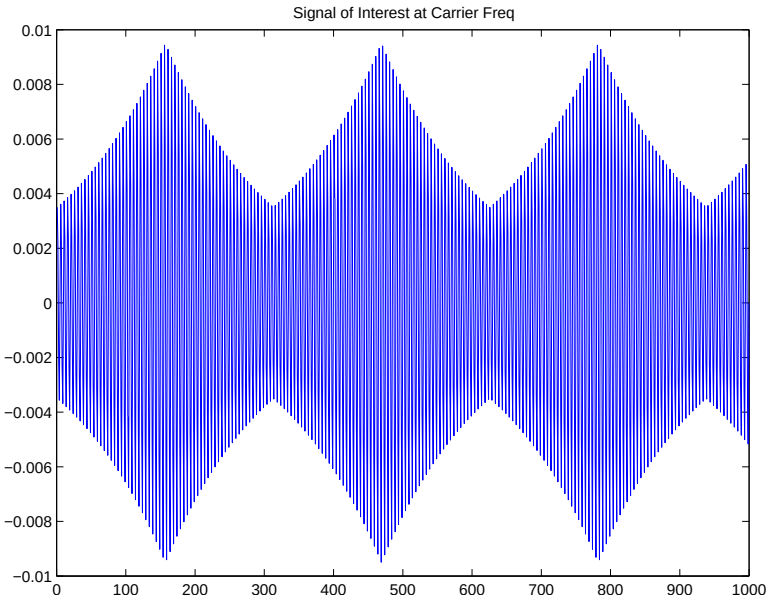

Figure 4.27: Plot of the signal of interest at the carrier frequency.

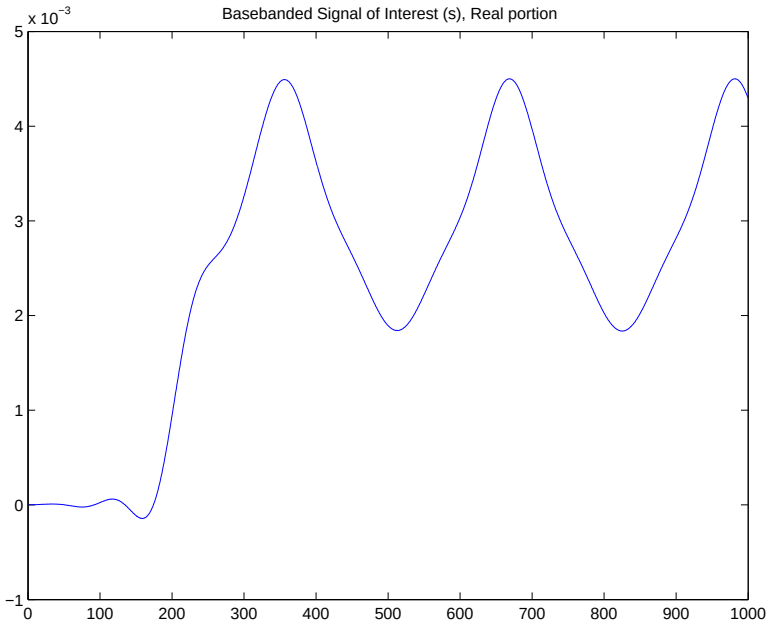

Figure 4.28: Plot of the base-banded version of the signal of interest. This is the envelope of the signal, s, added to the primary channel.

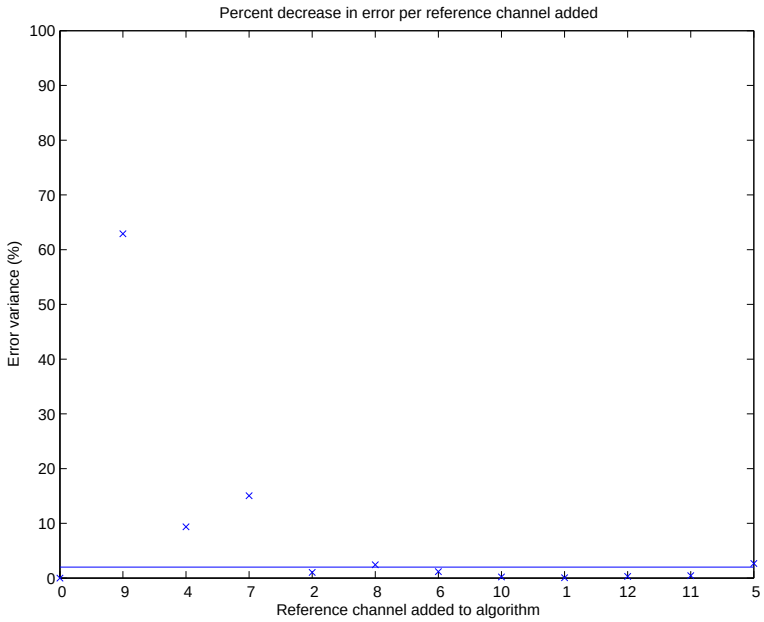

Figure 4.29: Plot of the marginal improvement for each reference channel along with a horizontal line marking the 2% threshold.

channel be below the threshold when subsequent reference channels contribute significantly. This previously described criteria would not count those subsequent channels. This case can be seen in Figure 4.19 where marginal improvement using the last channel, number five, is significant while that of the previous six to eight channels is not.

A different criteria is proposed to deal with this case. $\hat{K}_{VRAC}$ is set to the total number of channels used in the adaptive beamforming algorithm that have a marginal improvement above a specified threshold. As an example, Figure 4.29 shows the marginal improvement for each reference channel with a horizontal line that marks a threshold of 2%. The first criteria puts $\hat{K}_{VRAC}$ at three while the second criteria gives five as the value for $\hat{K}'_{VRAC}$.

Another consideration is which threshold value to use. The value should be large enough to only include channels that significantly improve the estimate of s. Some of the preliminary analysis results show that almost all of the reference channels

reduce the error by at least one to two percent, a reduction that is quite insignificant compared to those of the first few reference channels. A threshold in the range of two to five percent will count most of the channels that have a significant contribution and ignore those that are simply counteracting the effects of white noise.

Chapter 5

Analysis Results

With the foundation given in Chapter 4, the data acquired from the field experiments can be analyzed. These results help answer the questions posed in Section 4.1: how many reference channels are needed to effectively cancel out the RFI, how many interfering signals are present, what spacing should the reference antennas have, and what bandwidth should be in the RFI mitigation system? This chapter presents results from the data analysis that address these questions.

Since the data acquisition system was improved after the first field experiment to have much better channel balance, backup channels, and better control of clipping, the results presented here are all taken from this second field trial. 199 one minute data frames were collected. Data was collected for one out of every 10 minutes as described in section 3.2. Sampling began at 9:45 PM on Thursday the 19th of September and ended at approximately 7:50 AM on Saturday the 21st. During this experiment there was a period when the signal levels at the output of the receiver boards were greater than the input limits on the A/D converter. The data collected during this window (data frames 63 through 122) is severely clipped. Any results from this portion of the data are possibly invalid due to the data distortion, and are not emphasized in this report.

5.1 VRAC Results

The VRAC algorithm results provide a direct indication of how many reference antennas are needed to effectively cancel out the RFI. As mentioned in Chapter 4, parameter settings for VRAC which produced the best analysis results are: 10 second

blocks, reference channels ordered by correlation coefficient ranking, channels three and six used as primary channels, and a threshold of two to five percent.

First the results using a threshold of 2% will be presented. Figure 5.1 shows the mean $\hat{K}_{VRAC}$ values computed for each data frame that did not contain a calibration signal with channel three used as the primary channel. For each data frame $\hat{K}_{VRAC}$ was computed for each 10 second block. The mean was taken over the six $\hat{K}_{VRAC}$ values per frame. Data frames containing a calibration tone were not used because the corresponding $\hat{K}_{VRAC}$ values were not valid due to the very strong calibration tone. These frames were excluded from the plot. Figures 5.2 and 5.3 show the minimum and maximum $\hat{K}_{VRAC}$ for each data frame.

The results for a 2% threshold and channel three as the primary channel show that on average 4.1 reference channels are needed to cancel out the interference and that as many as nine can be useful, although the average maximum value is 5.1. The average minimum $\hat{K}_{VRAC}$ value is 1.9. Frames with calibration signals were excluted when computing these statistics.

Figures 5.4, 5.5, and 5.6 show the mean, minimum, and maximum $\hat{K}_{VRAC}$ plots, respectively, when channel six is the primary channel. As before, the block size is 10 seconds, a threshold of 2% is used, and the frames with a calibration tone were excluded. These results show that on average 3.4 reference channels are needed to cancel out the interference and that as many as eight can be useful, with 3.9 as the average maximum. The average minimum $\hat{K}_{VRAC}$ value is 1.9.

The results for a 5% threshold will now be presented. Figures 5.7, 5.8, and 5.9 show the mean, minimum, and maximum $\hat{K}_{VRAC}$ over each data frame with 10 second blocks and channel three as the primary channel. Figures 5.10, 5.10, and 5.10 show the mean, minimum, and maximum $\hat{K}_{VRAC}$ values for the same settings with channel six as the primary channel. For channel three as the primary channel, the average $\hat{K}_{VRAC}$ value is 2.5. The maximum $\hat{K}_{VRAC}$ value is 6 and the average maximum is 3.3. The average minimum value is 1.7. For channel 6 as the primary channel, the average $\hat{K}_{VRAC}$ value is 2.2. The maximum $\hat{K}_{VRAC}$ value is five and the

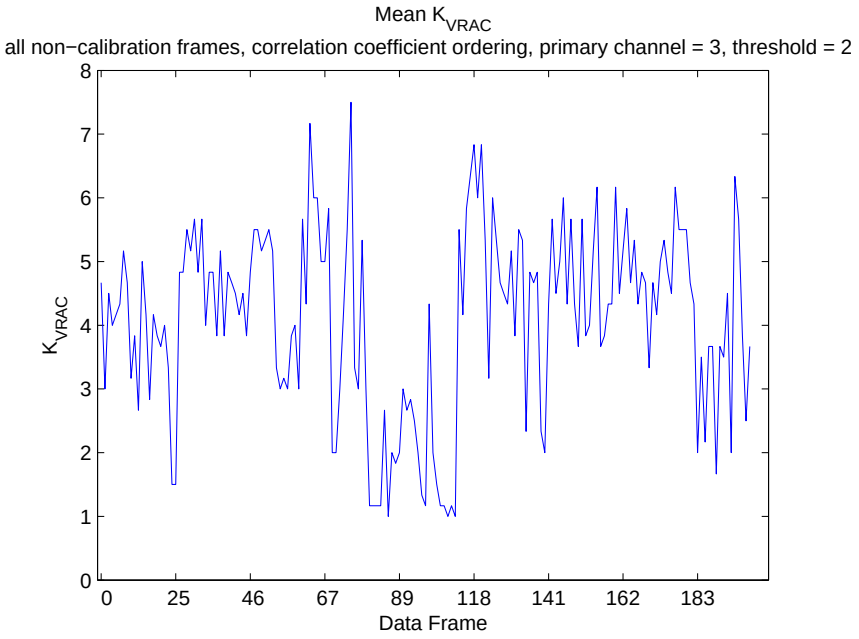

Figure 5.1: Plot of mean $\hat{K}_{VRAC}$ for primary channel three with a threshold of 2%. Data frames with a calibration tone were excluded.

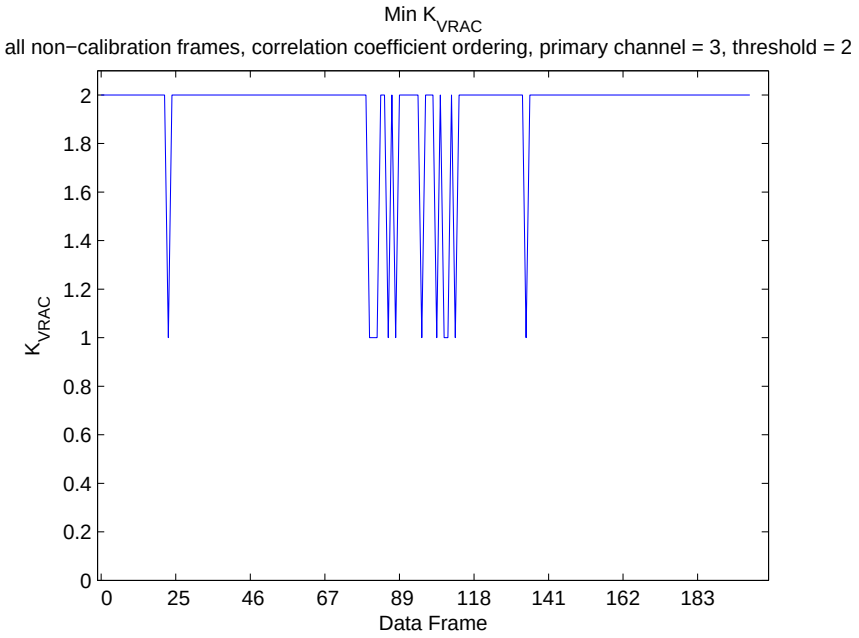

Figure 5.2: Plot of minimum $\hat{K}_{VRAC}$ for primary channel three with a threshold of 2%. Data frames with a calibration tone were excluded.

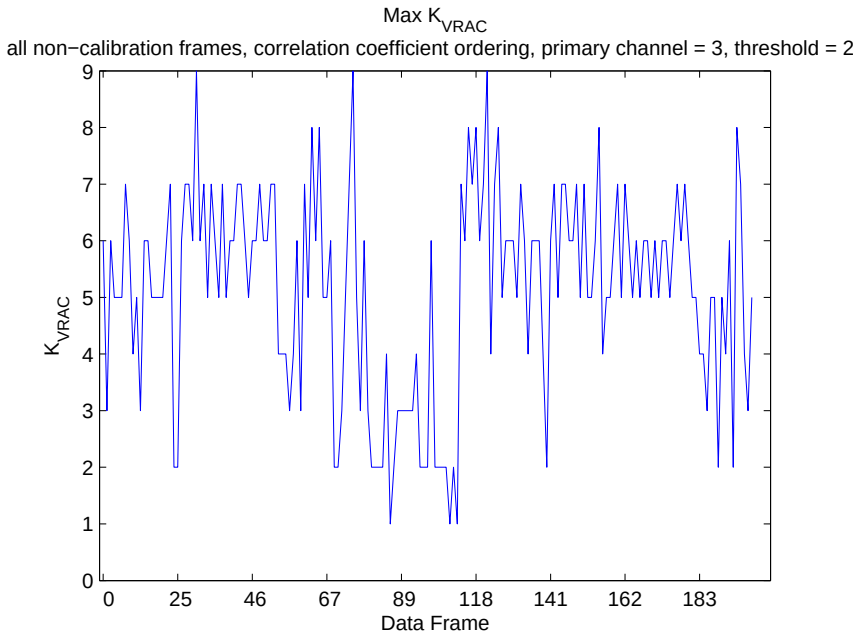

Figure 5.3: Plot of maximum $\hat{K}_{VRAC}$ for primary channel three with a threshold of 2%. Data frames with a calibration tone were excluded.

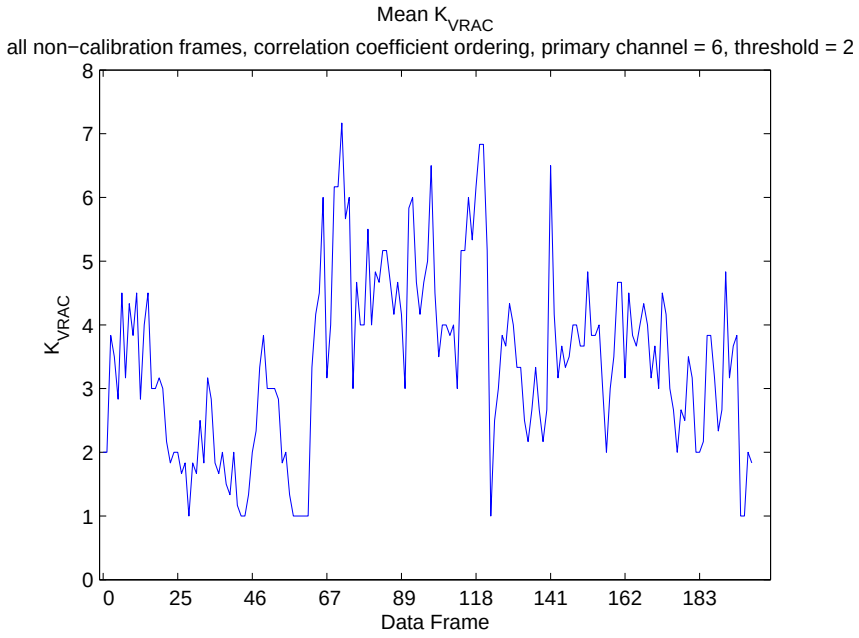

Figure 5.4: Plot of mean $\hat{K}_{VRAC}$ for primary channel six with a threshold of 2%. Data frames with a calibration tone were excluded.

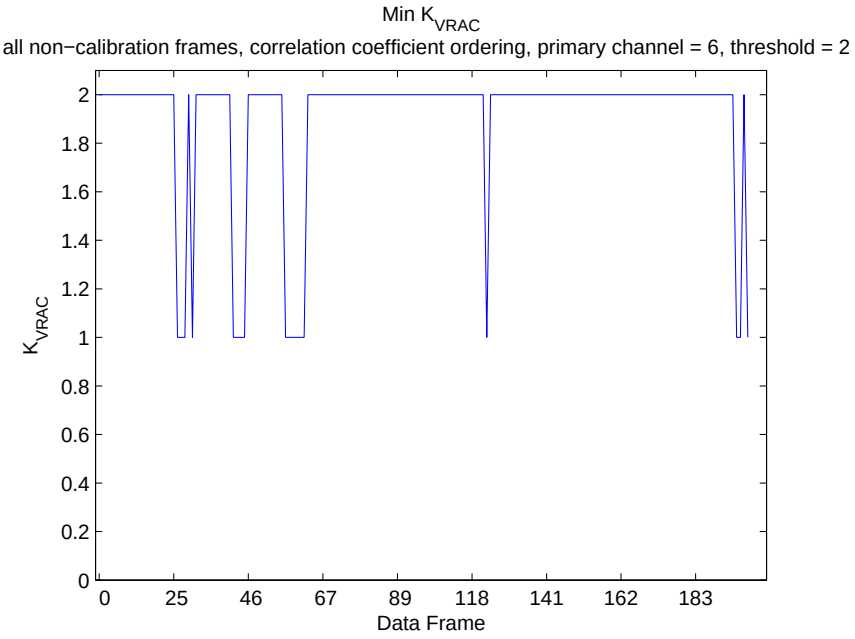

Figure 5.5: Plot of minimum $\hat{K}_{VRAC}$ for primary channel six with a threshold of 2%. Data frames with a calibration tone were excluded.

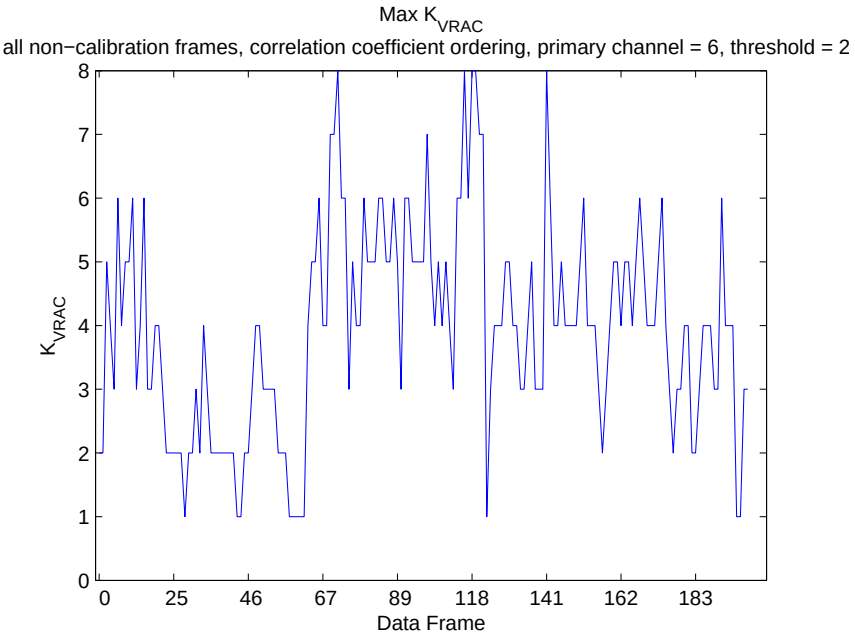

Figure 5.6: Plot of maximum $\hat{K}_{VRAC}$ for primary channel six with a threshold of 2%. Data frames with a calibration tone were excluded.

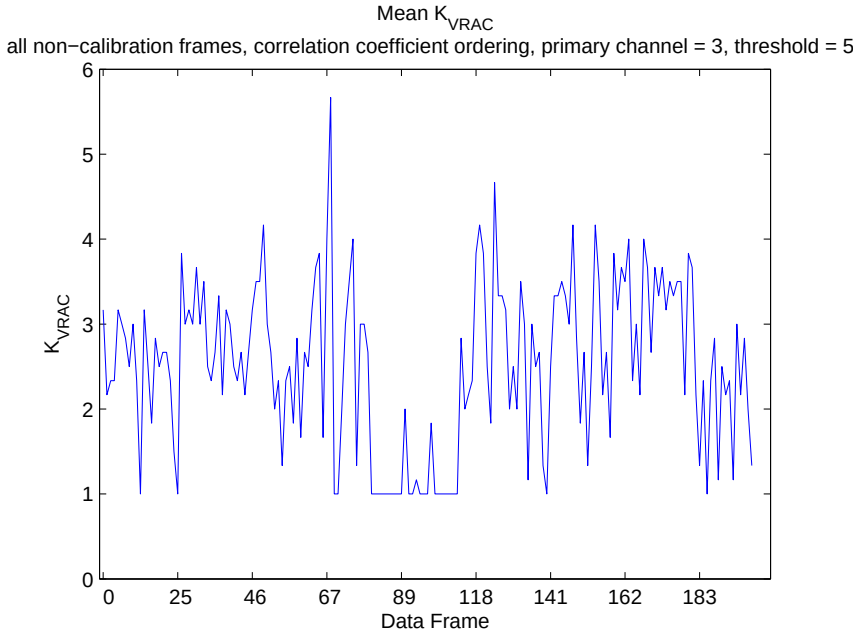

Figure 5.7: Plot of mean $\hat{K}_{VRAC}$ for primary channel three with a threshold of 5%. Data frames with a calibration tone were excluded.

average maximum is 2.5. The average minimum value is 1.8. A summary of all the results thus far is given in table 5.1.

The $\hat{K}_{VRAC}$ results for a threshold of 5% percent are, as expected, significantly lower than those for a threshold of 2%. Given that the mine detection application is cancelling out RFI to detect very low level NQR signals, the results for the more aggresive threshold of 2% will be emphasized.

Figures 5.13 and 5.14 show the minimum percent $var(\epsilon_{min})$ achieved for each data with channels three and six as the primary channels, respectively. The average values are 6.8 and 7.9%, meaning that on average, the adaptive beamforming algorithm was able to cancel out 93.2 and 92.1% of the original error power for channels three and six, respectively.

Figures 5.15 and 5.16 show the average SINR improvment achieved for channels three and six as the primary channels, respectively. In these plots, all 11 reference channels were used in the MSC algorithm. The average improvment was 13.3 dB for

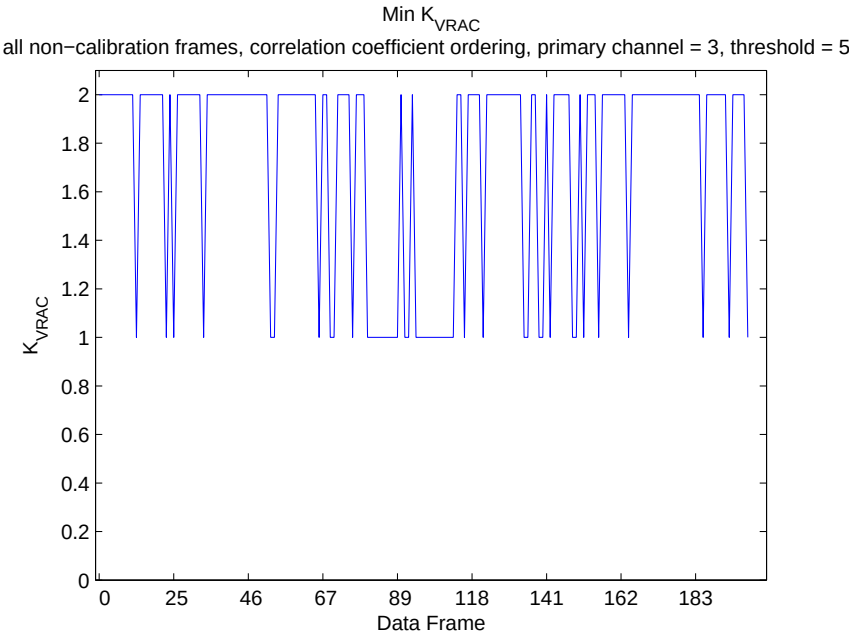

Figure 5.8: Plot of minimum $\hat{K}_{VRAC}$ for primary channel three with a threshold of 5%. Data frames with a calibration tone were excluded.

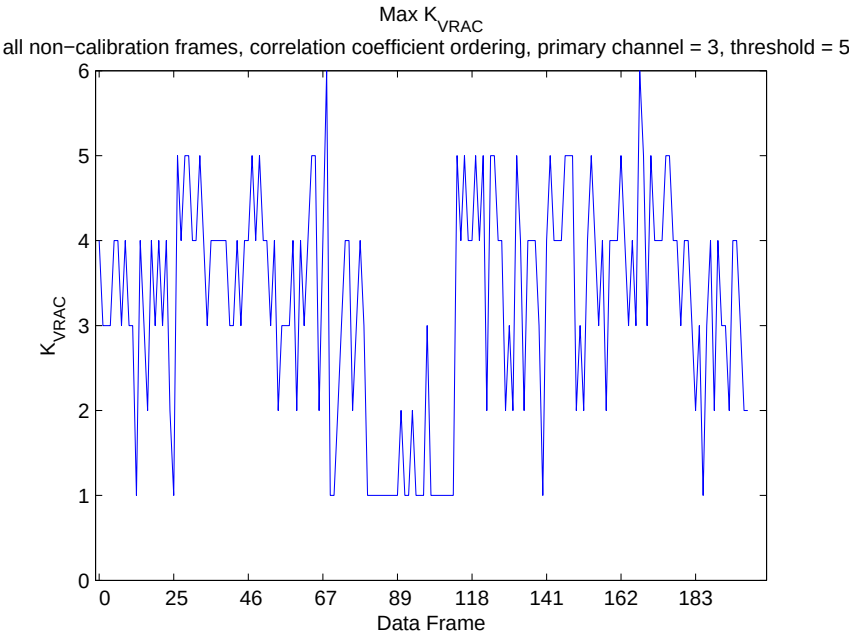

Figure 5.9: Plot of maximum $\hat{K}_{VRAC}$ for primary channel three with a threshold of 5%. Data frames with a calibration tone were excluded.

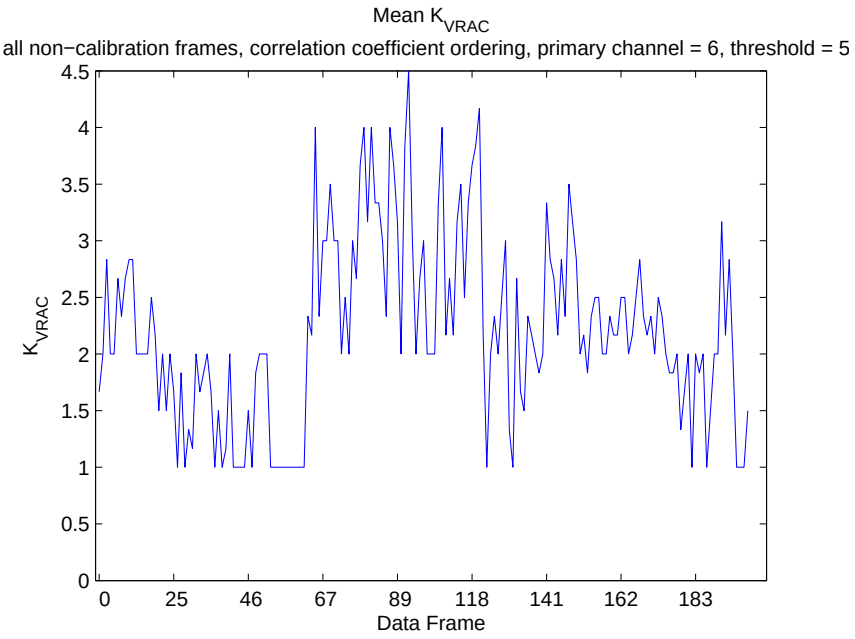

Figure 5.10: Plot of mean $\hat{K}_{VRAC}$ for primary channel six with a threshold of 5%. Data frames with a calibration tone were excluded.

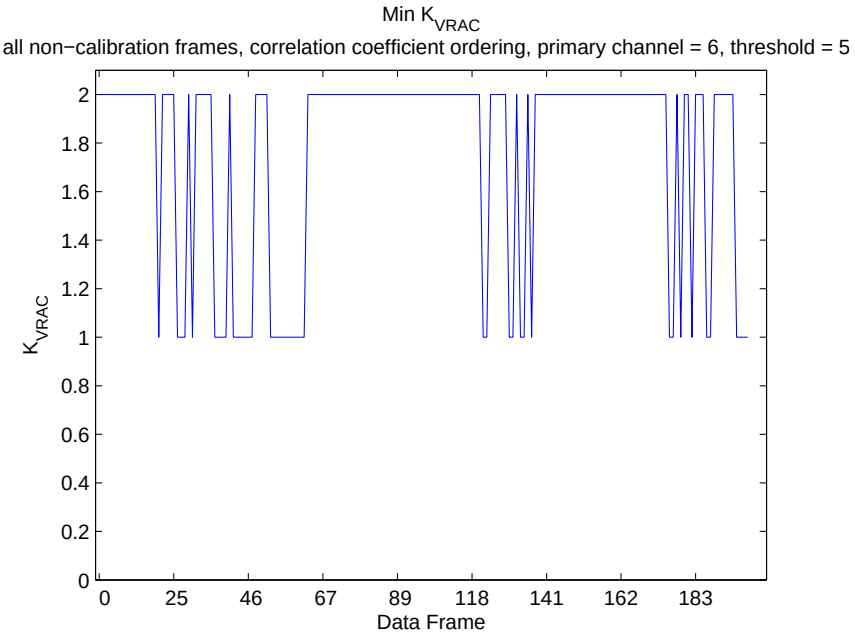

Figure 5.11: Plot of minimum $\hat{K}_{VRAC}$ for primary channel six with a threshold of 5%. Data frames with a calibration tone were excluded.

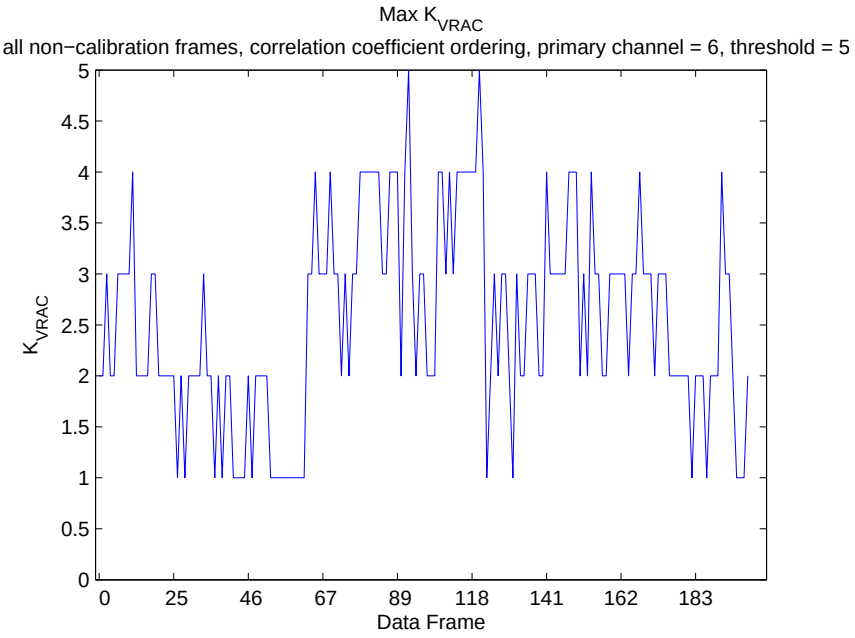

Figure 5.12: Plot of maximum $\hat{K}_{VRAC}$ for primary channel six with a threshold of 5%. Data frames with a calibration tone were excluded.

Table 5.1: Summary of $\hat{K}_{VRAC}$ results

Settings		$\hat{K}_{VRAC}$ Value			
Primary Channel	*Threshold*	*Average Min*	*Average*	*Average Max*	*Max*
3	2%	1.9	4.1	5.1	9
	5%	1.7	2.5	3.3	6
6	2%	1.9	3.4	3.9	8
	5%	1.8	2.2	2.5	5

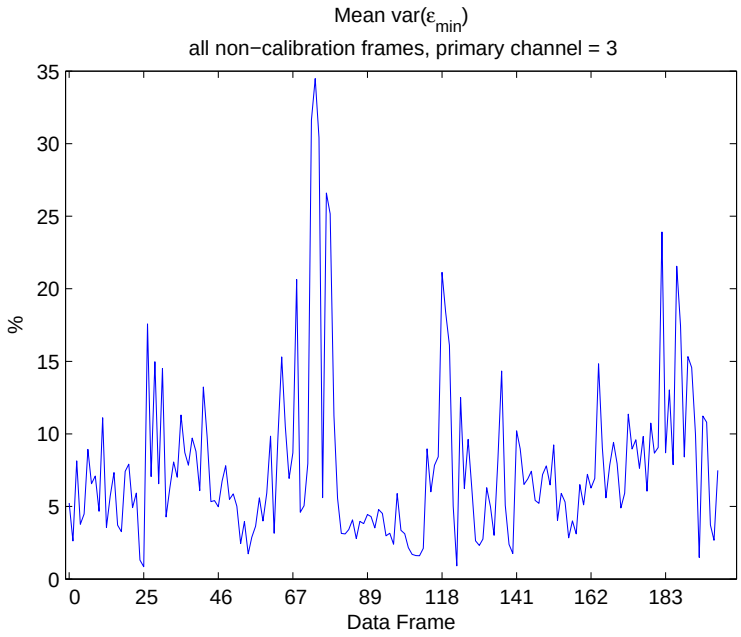

Figure 5.13: Plot of the average $var(\epsilon_{min})$ for channel 3 as the primary channel. Data frames with a calibration tone were excluded.

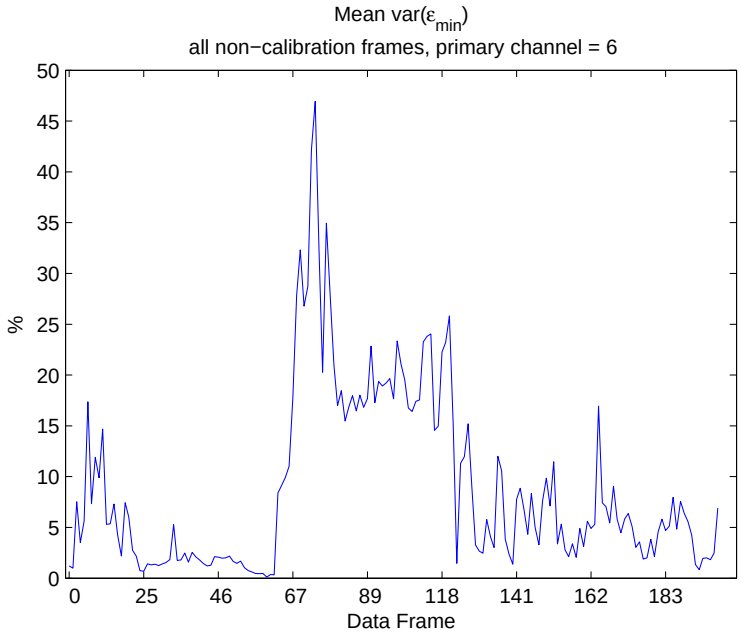

Figure 5.14: Plot of the average $var(\epsilon_{min})$ for channel 6 as the primary channel. Data frames with a calibration signal were excluded.

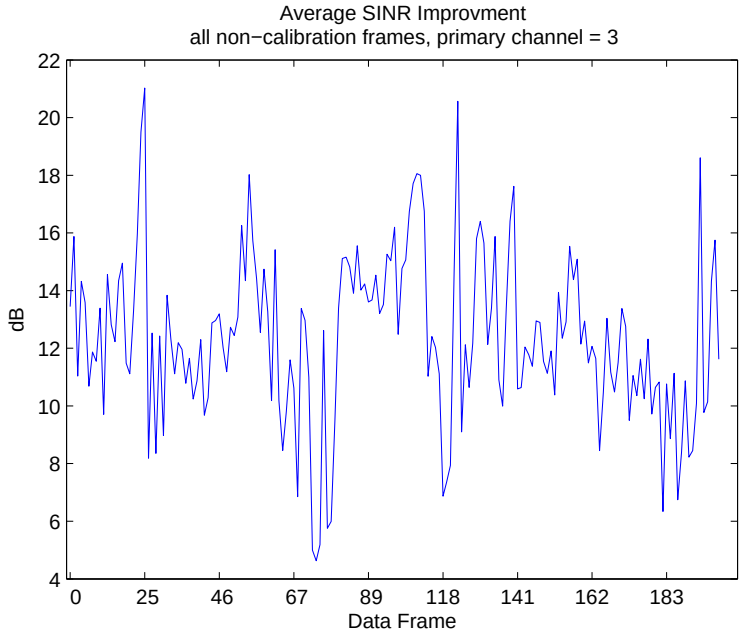

Figure 5.15: Plot of the average SINR improvment for channel 3 as the primary channel when all 11 reference channels were used in the adaptive cancellation. Data frames with a calibration tone were excluded.

channel three as the primary channel and 16.1 dB for channel 6 as the primary channel.

As was mentioned at the beginning of this chapter, the VRAC results of data frames 63 through 122 must be questioned due to clipping. One will notice in figures 5.1 through 5.12 that the results for these data frames are a little different than the rest. A simple visual inspection shows that for channel 3 as the primary channel the $\hat{K}_{VRAC}$ results tend to be lower in this region while those for channel 6 as the primary channel tend to be higher. The summary statistics presented in 5.1 were computed without the $\hat{K}_{VRAC}$ values from the data frames containing a calibration signal. In table 5.2 summary statistics are presented that were computed without either the results from data frames with calibration signals or clipping. These results are probably more reliable than those including clipped data.

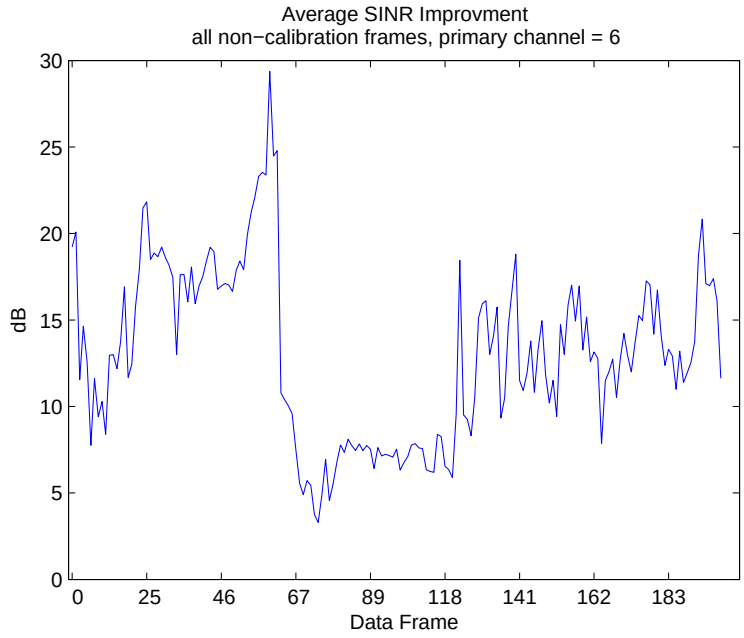

Figure 5.16: Plot of the average $var(\epsilon_{min})$ for channel 6 as the primary channel. Data frames with a calibration signal were excluded.

Table 5.2: Summary of $\hat{K}_{VRAC}$ results excluding clipped data

Settings		$\hat{K}_{VRAC}$ Value			
Primary Channel	*Threshold*	*Average Min*	*Average*	*Average Max*	*Max*
3	2%	2.0	4.4	5.4	9
	5%	1.8	2.7	3.6	6
6	2%	1.9	2.9	3.4	8
	5%	1.7	1.9	2.2	5

It should be noted that due to the directivity of the loop-stick antennas used in this experiment, the $\hat{K}_{VRAC}$ results included here probably do not represent the number of reference channels required to cancel out interference from all 360 degrees. Channels three and six were chosen as primary channels because of their signal quality and because they were oriented perpendicular to each other. The idea was that $\hat{K}_{VRAC}$ for each channel could be combined to determine the number of reference channels required to cancel out interference on an isotropic antenna. But, as noted in section 3.1, the windy conditions of the second field experiment caused the antennas to rotate. Therefore, it is unlikely that the antennas for channels 3 and 6 were perpendicular to each other at the end of the experiment. Therefore, the results for each channel must be considered independently.

5.2 Number of Interferers and Reference Antenna Spacing

As described in Section 4.3.2, the VRAC algorithm cannot estimate the number of interfering signals present in the data. Therefore, the results of the data analysis using the VRAC algorithm do not answer this question. Even if the number of interferers were known, this information would only be useful in a practical way if it determines the number of reference antennas needed to cancel out the RFI. Since VRAC does give us this answer, the fact that the actual number of interferers is unknown is a small loss.

There was no evidence that antenna spacing larger than 1/4 wavelength made RFI cancelation more effective. In examining how effective each reference channel was at canceling out RFI, there was no correlation with the distance from the primary channel. Performance for antennas spaced less than 1/4 wavelength away from the primary channel was not investigated.

5.3 Interferer Bandwidth

In all the analysis thus far, in the primary and reference channels were low pass filtered at 10 kHz before computing statistics and applying the adaptive beamforming algorithm. The signal of interest is inherently narrowband so constraining the RFI

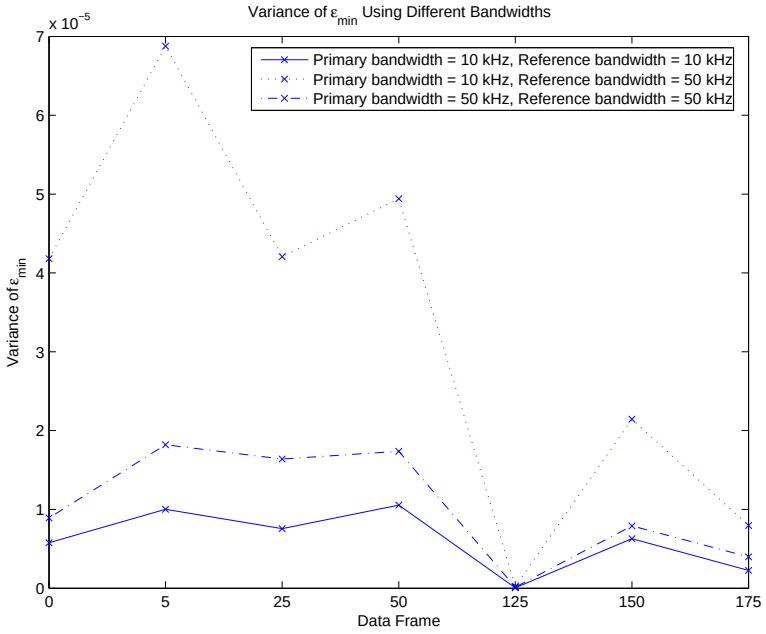

Figure 5.17: Plot of the variance of ϵ_{min} calculated from the first 10 second block of several data frames. The solid line shows the results from the standard setup, with a 10 kHz bandwidth for the reference channels. The dashed line shows the results using a 50 kHz bandwidth for the reference channels.

mitigation algorithm to work on a narrow band is logical. However, including a wider bandwidth of interferer information from the reference channels might help cancel out even more RFI if carriers outside the band of interest introduce low level spectral sidelobe components in the desired signal band. In order to test this, the adaptive beamformer was run using a 10 kHz bandwidth for the primary channel and a 50 kHz bandwidth for the reference channels. Figure 5.17 shows a comparison of the performance using both bandwidths for the reference channels. The 10 kHz bandwidth does much better in every data frames tested. This indicates that the narrower bandwidth is the best choice.

5.4 Summary of Results

This analysis shows that at least three or four reference channels should be used in an RFI cancelation system to ensure good performance on average. Since

the VRAC algorithm determined that up to eight or nine reference antennas were useful, additional reference channels would help ensure good performance in more RFI environments. Also, because the primary and reference antennas are directive, more reference antennas would probably be needed to cancel out RFI for a isotropic primary antenna.

Narrower bandwidths in the RFI mitigation system appear to perform better than wider. Including information from interfering signals that do not have a strong presence at the frequency of interest did not contribute much to RFI mitigation. Also, the additional information appeared to prevent the adaptive beamformer from effectively estimating the statistics of the signals that interfered most with the signal of interest. So, instead of improving performance, the wider bandwidth actually decreased performance.

Chapter 6

Conclusion

This thesis presents the successful results of a research project to study the RFI environment at frequencies specific to NQR based land mine detection. In spite of challenges encountered during the platform development, field experiments, and data analysis, usable estimates were obtained for the number of reference channels required in an RFI mitigation system to effectively cancel out interference. Though one must be cautions in generalizing the results we obtained from a specific location on two specific days, we do believe this data is representative of a typical a.m. radio broadcast interference environment.

It was shown that at least three or four reference channels should be used in an RFI cancellation system to ensure good performance on average. More may be required to insure acceptable cancellation in more difficult signal environments. It is notable that there is wide variation over time in the required number of channels to achieve acceptable interference rejection. This indicates that the interference environment is dynamic, with signal rank and spatial structure varying rapidly. A successful canceller design may need seven to nine reverence channels to insure reliable interference rejection over several hours. Improvements were realized with up to nine reference antennas in most signal conditions, but contribution of the last two to four antennas were relatively small.

Narrower bandwidths in the RFI mitigation system appear to perform better than wider. Including information from interfering signals that do not have a strong presence at the frequency of interest did not contribute much to RFI mitigation. Also, the additional information appeared to prevent the adaptive beamformer from

effectively estimating the statistics of the signals that interfered most with the signal of interest. So, instead of improving performance, the wider bandwidth actually decreased performance. The 10 kHz bandwidth performed much better in every data frame tested. This indicates that the narrower bandwidth is the best choice.

There was no evidence that antenna spacing larger than 1/4 wavelength made RFI cancellation more effective. This is an important observation which rejects one hypothesis on how canceller performance could be improved. We had originally proposed that for the NQR mine detection system, placing reference antennas on separate vehicles at some longer distance could improve canceller performance. The thinking was that at these long wavelengths there would be significant spatial information that could only be exploited if sensor spacing was some large fraction of a wavelength. These experiments have shown that such an extended auxiliary antenna geometry would not likely help. Variation in effectiveness of antennas spaced less than 1/4 wavelength away from the primary channel was not investigated.

Though signal levels differed significantly between daytime and nighttime data sets (i.e. much higher levels at night) we saw no clear day-night variation in the number of required reference antennas, $\hat{K}_{VRAC}$. This could be characteristic of the specific test site location due to the operational practices of regional broadcast stations and may not be true at other test sites.

Finally we note that only horizontally polarized B-field loop stick antennas were used in this experiment. The array included a variety of orientations in azimuth for these bi-direction response antennas, but no vertical polarization. It would be advisable to repeat these experiments with a mixture of B-field and E-field (e.g. dipole) antennas and with three orthogonal axes of polarization.

Bibliography

[1] R. Siegel, "Land mine detection", *IEEE Instrumentation and Measurement Magazine*, pp. 22–28, December 2002.

[2] J. A. S. Smith, "Nitrogen-14 quadrupole resonance detection of rdx and hmx based explosives", in *European Convention on Security and Detection*. 1995, number 408, IEE.

[3] A. N. Garroway, M. L. Buess, J. B. Miller, B. H. Suits, A. D. Hibbs, G. A. Barrall, R. Matthews, and L. J. Burnett, "Remote sensing by nuclear quadrupole resonance", *IEEE Transactions on Geoscience and Remote Sensing*, vol. 39, June 2001.

[4] Moon and Stirling, *Mathematical Methods and Algorithms for Signal Processing*, chapter 3, Prentice Hall, 2000.

[5] D. Pulsipher, S. Boll, C. Rushforth, and L. Timothy, "Reduction of nonstationary acoustic noise in speech using lms adaptive noise cancelling", in *IEEE International Conference on Acoustics, Speech, and Signal Processing*. ICASSP '79, April 1979, vol. 4, pp. 204–207.

[6] N. L. Owsley, *Array Signal Processing*, chapter 3, Prentice-Hall, 1985.

[7] B. D. Jeffs, L. Li, and K. F. Warnick, "Auxiliary antenna-assisted interference mtigation for radio astronomy arrays", *IEEE Transactions on Signal Processing*, vol. 53, no. 2, pp. 439–451, Feb 2005.

[8] M. H. Hayes, *Statistical Digital Signal Processing and Modeling*, chapter 9, John Wiler & Sons, Inc., 1996.

[9] Y. Tan, S. L. Tantum, and L. M. Collins, "Landmine detection with nuclear quadrupole resonance", in *Geoscience and Remote Sensing Symposium, 2002.* IGARSS '02, 2002, vol. 3, pp. 1575–1578, IEEE International.

[10] B. D. Van Veen and K. M. Buckley, "Beamforming: A versatile approach to spatial filtering", in *IEEE ASSP Magazine*, Apr 1988, vol. 5, pp. 4–24.

[11] H. L. Van Trees, *Optimum Array Processing*, chapter 7, Wiley-Interscience, 2002.

[12] M. Wax and T. Kailath, "Detection of signals by information theoretic criteria", in *IEEE Transactions on Acoustic, Speech, and Signal Processing*, April 1985, vol. ASSP-33, pp. 387–392.

[13] H. Akaike, "Infomration theory and an extension of the maximum likelihood principle", in *Proceedings of the Second International Symposium on Information Theory, Supplement to Problems of Control and Information Theory*, 1972, pp. 267–28.

[14] H. Akaike, "A new look at the statistical model indentification", in *IEEE Transactions on Automatic Control*, December 1985, vol. AC-19, pp. 716–723.

[15] G. Schwartz, "Estimating the dimension of a model", *Annals of Statistics*, vol. 6, pp. 461–464, 1978.

[16] J. Rissanen, "Modelling by shortest data description", *Automatica*, vol. 14, pp. 465–471, 1978.

[17] A. S. Sekmen and Z. Bingul, "Comparison of algorithms for detection of the number of signal sources", in *Southeastcon '99. Proceedings. IEEE*, March 1999, pp. 70–73.

[18] Q. Zhang, K. M. Wong, P. C. Yip, and J. P. Reilly, "Statistical analysis of the performance of information theoretic criteria in the detection of the number of

signals in array processing", *IEEE Transactions on Acoustics, Speech, and Signal Processing*, vol. 37, no. 10, pp. 1557–1567, October 1989.

[19] R. D. Straw, Ed., *The ARRL Antenna Book*, chapter 5, ARRL, 19th edition, 2000-2002.